



Prolonged La Niña events and the associated heat distribution in the Tropical Indian Ocean

Soumya Mukhopadhyay¹ · C. Gnanaseelan¹ · Jasti S. Chowdary¹ · Anant Parekh¹ · Sandeep Mohapatra^{1,2}

Received: 19 April 2021 / Accepted: 11 October 2021

© The Author(s), under exclusive licence to Springer-Verlag GmbH Germany, part of Springer Nature 2021

Abstract

In the present study, heat redistribution in the Tropical Indian Ocean (TIO) associated with the prolonged La Niña events during 1958–2017 is examined using reanalysis/observations. It is found that the prolonged La Niña forcing strengthened the east–west thermocline gradient in the equatorial Indian Ocean and propelled the eastward extension of thermocline ridge of the Indian Ocean (TRIO) from its climatological location of southwestern TIO. The cyclonic winds over the southeastern TIO and the associated upwelling Rossby waves are primarily driving the TRIO intensification and its eastward extension. Anomalous subsurface warming, thermocline deepening, and the associated increase in the upper ocean heat content and sea-level in the eastern equatorial Indian Ocean, southeastern TIO and Bay of Bengal (BoB) are found to be the characteristic features of the prolonged La Niña events. Cross equatorial Sverdrup transport near the eastern boundary during the prolonged La Niña events has increased the heat content of BoB and is found to be a pathway of Pacific water entering the north Indian Ocean.

Keywords North Indian Ocean · Upper ocean heat content · Sverdrup transport · Cross equatorial flow · Sea-level variations

1 Introduction

El Niño–Southern Oscillation (ENSO) is the most prominent interannual mode of climate variability. It influences the Indian Ocean via the heat fluxes (Klein et al. 1999; Alexander et al. 2002) and ocean dynamics (e.g., Masumoto and Meyers 1998; Chowdary and Gnanaseelan 2007). The Tropical Indian Ocean (TIO) surface and subsurface temperature are modulated by ENSO (e.g. Du et al. 2009, 2013; Singh et al. 2013; Sayantani and Gnanaseelan 2015). The rapid Indian Ocean warming (Nieves et al. 2015; Lee et al. 2015) and associated sea-level rise (Thompson et al. 2016; Srinivasu et al. 2017) in the early twenty-first century have coincided with the global warming “hiatus” (e.g. Meehl et al. 2011; England et al. 2014). This early twenty-first century hiatus is primarily attributed to a “La Niña”

like negative phase of the Interdecadal Pacific Oscillation (IPO) and the associated surface easterlies along the equatorial Pacific (Kosaka and Xie 2013). These easterlies pile-up warm water in the western Pacific. Some of these warm waters are advected into the southern TIO (STIO) (Lee et al. 2015; Nieves et al. 2015; Liu et al. 2016; Zhang et al. 2018; Li et al. 2018, 2019) through Indonesian archipelago in the form of the Indonesian Through Flow (ITF) increasing the upper ocean heat content there (Wijffels and Meyers 2004). The increased ITF transport, cooled the top 100 m temperature of the west Pacific Ocean, whereas it was mostly compensated by the subsurface warming of Indian Ocean (100–300 m) in post 2000s (e.g., Nieves et al. 2015).

The La Niña events tend to enhance the ITF transport, responding to these easterlies over the equatorial Pacific (Meyers 1996; England and Huang 2005). ITF plays a central role in the heat budget of the Indo-Pacific region (Godfrey 1996). Using a HYCOM model, Li et al. (2018) have shown that ITF is primarily dictated by the Pacific trade winds which directly affects the STIO and affects the north Indian Ocean (NIO) through meridional heat transport of the western boundary current. In a classical La Niña (El Niño) event, a negative (positive) Sea Surface Temperature

✉ C. Gnanaseelan
seelan@tropmet.res.in

¹ Indian Institute of Tropical Meteorology, Ministry of Earth Sciences, Pune 411008, India

² Department of Atmospheric and Space Sciences, Savitribai Phule Pune University, Pune 411007, India

(SST) anomaly is seen in the eastern and central parts of the equatorial Pacific which persists for 12–18 months. But in prolonged or “protracted” ENSO events SST anomalies persist for more than 2-years or so (e.g., Allan and D’Arrigo 1999). Prolonged La Niña events induce anomalously strong Pacific–Indian Ocean pressure gradient (England et al. 2014), which strengthens the easterly trade winds over the equatorial Pacific and contributes to the enhanced ITF transport (e.g., Lee et al. 2015).

The upper ocean heat content (UOHC) is an important parameter in the STIO region as it modulates the SST, sea-level anomaly (SLA) and the ocean–atmosphere interactions (e.g., Xie et al. 2002). They are influenced significantly by the local forcing of the Indian Ocean (e.g., Wyrski 1973; Saji et al. 1999). For example, in the eastern equatorial Indian Ocean (EEIO) region, UOHC is high during monsoon transition months (May and November) (Wyrski 1973, Hastenrath 1993) compared to other months. The equatorial currents (Yoshida jet/Wyrski jet) and the eastward propagating downwelling Kelvin waves are dominant in the equatorial Indian Ocean (EIO) (5° S–5° N, 90° E–100° E) during the monsoon transition periods or months (April–May and October–November). These downwelling Kelvin waves enhance UOHC in EIO through mass convergence and depression of the thermocline (Wyrski 1973). On the other hand, low UOHC of top 300 m is observed in the southwestern TIO throughout the year. This is due to Ekman divergence associated with the clockwise (cyclonic) gyre. During the summer monsoon, the UOHC is maximum in the central Arabian Sea due to deeper surface mixed layer (Rao 1986) and the deepening of thermocline is induced by negative wind stress curl (Hastenrath and Lamb 1979) in the region south of the Somali jet core.

More than El Niño, La Niña forcing could induce strong subsurface warming over the EIO region (Srinivas et al. 2018), suggesting the possible influence of La Niña or prolonged La Niña events on TIO variability. It is well known that Pacific Ocean variability modulates Indian Ocean conditions on interannual (e.g. Xie et al. 2009; Sreenivas et al. 2012; Deepa et al. 2018) and decadal time scales (e.g. Han et al. 2014; Deepa et al. 2019). The inter-annual and decadal variability of UOHC and sea-levels are closely linked with each other because of thermal expansion and connected through the ocean transports (Verschell et al. 1995; Masumoto and Meyers 1998; Birol and Morrow 2001; Wijffels and Meyers 2004; Trenary and Han 2012; Li et al. 2018; Zhang et al. 2019).

Despite of several studies addressing cooling or warming patterns/trends in TIO, it remains unclear how much of the UOHC changes in the TIO are associated with the prolonged La Niña events. So, in this paper, we use ocean reanalysis data to quantify the UOHC as well as sea-level variability in TIO during the prolonged La Niña events. We have used data from

1958 to 2017 to better capture the natural variability. The data sources are described in Sect. 2. The prolonged La Niña events and the associated SST and wind patterns in the Indo-Pacific basins and vertical temperature profiles, spatial variations of the heat content etc. are described in Sect. 3. The volume, and meridional Sverdrup transport, the analysis of the UOHC and Sea Surface Height (SSH) are described in Sect. 4, the summary and discussion of the results are given in Sect. 5.

2 Data and methods

The Ocean Reanalysis System 4 (ORAS4) data (Balmaseda et al. 2013) during 1958–2017 is used in this study. The ORAS4 has been identified as the best reanalysis product for the Indian Ocean region compared to other widely used available reanalysis products (Karmakar et al. 2018). Anomalies are calculated after detrending the data for the given duration. Parzen smoother is used to obtain running mean and Lanczos filter is used to low-pass filter the data. Parzen smoother uses Parzen window to smooth the variable along the indicated axis. It is a nonparametric method for estimating continuous density function from the data and it uses weighted mean of neighbouring points along the indicated axis instead of equal weights.

ORAS4 zonal and meridional velocity fields, SSH and vertical temperature profiles are used to calculate the transports and UOHC. ORAS4 employs the variational ocean data assimilation system NEMOVAR using Nucleus for European Modelling of the Ocean (NEMO) version 3.0 ocean model. The vertical velocities from ORAS3 are used here as they are not provided in ORAS4. The UOHC is computed as follows:

$$UOHC = \rho_0 C_p \int_{d_1}^{d_2} T(z) dz \quad (1)$$

where $C_p = 4185 \text{ J Kg}^{-1} \text{ K}^{-1}$ is the specific heat capacity of the sea water and $\rho_0 = 1025 \text{ kg m}^{-3}$ is the reference sea water density, $T(z)$ is the vertical profile of potential temperature and d_1, d_2 are the corresponding reference depths.

Further meridional heat transport (MHT) is computed as follows:

$$MHT = \rho_0 C_p \int_{d_1}^{d_2} v(z) T(z) dz \quad (2)$$

The Wind Stress Curl (WSC) is estimated from the following equation

$$WSC = \frac{\partial \tau^y}{\partial x} - \frac{\partial \tau^x}{\partial y} \quad (3)$$

where $\tau^x = \rho_a C_d W_m U_{10}$ and $\tau^y = \rho_a C_d W_m V_{10}$ are the zonal and meridional wind stress. U_{10}, V_{10} are respectively the zonal and meridional winds at 10 m from ERA and JRA55,

W_m is the wind speed, $\rho_a = 1.25 \text{ kg m}^{-3}$ is density of air, ρ_0 is the density of ocean water. The drag co-efficient or momentum transfer co-efficient is wind dependent as in Parekh et al. (2011), they have computed the drag co-efficient over the NIO using ~40,000 in-situ observation from the region and has given formula corresponding to different wind speed range, which are as follows:

$$C_d = \begin{cases} 0.0011 * WS^{-0.1475} & \text{if } 0 \leq WS < 3.75 \text{ ms}^{-1} \\ 0.00005 * WS + 0.0008 & \text{if } 3.75 \leq WS < 18 \text{ ms}^{-1} \\ 0.00004 * WS + 0.0009 & \text{if } WS \geq 18 \text{ ms}^{-1} \end{cases} \quad (4)$$

Near the equator the cross equatorial Sverdrup transport is mainly dictated by the zonal wind stress curl component (Miyama et al. 2003). The formula for the meridional Sverdrup transport at the equator (equatorial belt) is as follows:

$$Sv \approx -\frac{1}{\beta \rho_0} \int_{x_w}^{x_e} \frac{\partial \tau^x}{\partial y} dx \quad (5)$$

where $\beta = \frac{\partial f}{\partial y}$ and f are the Rossby and Coriolis parameters respectively, x_e and x_w are the eastern and western boundaries where the wind stress curl is integrated for calculating the transport.

The contribution of zonal advection (of the heat budget) on the temperature can be estimated as follows.

$$zonal_{advection} = -\left[\bar{u} \frac{\partial \bar{T}}{\partial x} + \bar{u}' \frac{\partial T'}{\partial x} + u' \frac{\partial \bar{T}}{\partial x} \right] \quad (6)$$

where T = potential temperature and u = zonal current \bar{u}, u', \bar{T}, T' represents respectively the mean and anomalies of zonal current and potential temperature.

3 Surface and sub-surface temperature and heat content variability during prolonged La-Niña

The prolonged La Niña events are defined as the La Niña events which persisted for 24-months or more and is similar to the previous studies (e.g., Allan and D'Arrigo 1999; Reason et al. 2000; Allan et al. 2003). In this study, the prolonged La Niña events during 1958–2017 viz., 1973–1976, 1983–1986, 1998–2001, and 2010–2012 are subjected to detailed analysis. The above prolonged La Niña events are selected as they are the most persisting and prominent events in the equatorial Pacific. The list of prolonged and non-prolonged La Niña events with the durations are given in Table 1. To study the impact of persisting La Niña events on the TIO temperatures in spatial and vertical levels, we studied the time-depth section of anomalous temperature for different regions of TIO as well as spatial pattern of SST anomalies in the TIO (Figs. 1, 2). It is important to note that

Table 1 The list of pro-longed and non-prolonged La Niña events during 1958–2017 and their duration

Prolonged La-Niña events	Non prolonged La-Niña events
May 1973–May 1976 (37 months)	1964–1965 (10 months)
July 1983–May 1986 (35 months)	1970–1972 (21 months)
June 1998–December 2001 (43 months)	1988–1989 (14 months)
May 2010–April 2012 (24 months)	2007–2009 (21 months)

the prolonged La Niña events are selected based on three-month averaged time series of Niño3.4 index (Fig. 3). All the prolonged La Niña events considered for the study persisted for 24-months or more, which showed that the SST anomalies over the Niño3.4 region are less than -0.5 (green dashed line in the Fig. 3) for most of the period and it is more than 1 standard deviation ($SD = 0.83$) (red dashed line in Fig. 3) for significant part of the event. The prolonged La Niña events are shaded in beige in Fig. 3.

The anomalous vertical temperature profiles show that during all the prolonged La Niña events (marked by vertical black lines in Fig. 1), the maximum temperature variability is mostly confined to the 50–150 m depth levels (Fig. 1), though the signatures are found up to 300 m during some years (Fig. 1). Intense warming is seen in the east (Fig. 1b), whereas cooling is seen in the western region (Fig. 1c). The intensity of warming is stronger in the southeastern region (0° – 10° S), compared to the northeastern region (0° – 10° N) (figure not shown). However, mixed layer cooling is evident in this region during the prolonged La Niña events and is revealed in the basin wide SST pattern as well (Fig. 2). This clearly suggests that both surface and subsurface temperature distributions in the TIO are influenced by prolonged La Niña forcing. Motivated by changes in temperature, we have examined the factors that are responsible for upper ocean heat distribution in the TIO associated with the prolonged La Niña events. Hereafter heat content over 50–150 m is referred to as the subsurface heat content.

The composite of SST and wind anomaly during the persistent La Niña events is shown in Fig. 2. Anomalous cyclonic wind circulation covering the southern tropical Indian Ocean, maritime and Australian continents is a characteristic feature of prolonged La Niña events (Fig. 2a). This circulation is primarily responsible for the wind anomalies over EIO. Such cyclonic circulation is not evident during the La Niña events which are non-prolonged (Fig. 2b). The strength and longitudinal extent of the cyclonic circulation depends on the strength and extent of each prolonged La Niña associated cooling in the central and eastern equatorial Pacific. During 1998–2001 (strong long-lived) and 1983–1986 (moderate long-lived) La Niña events with the cold tongue of SST anomaly is mostly confined around

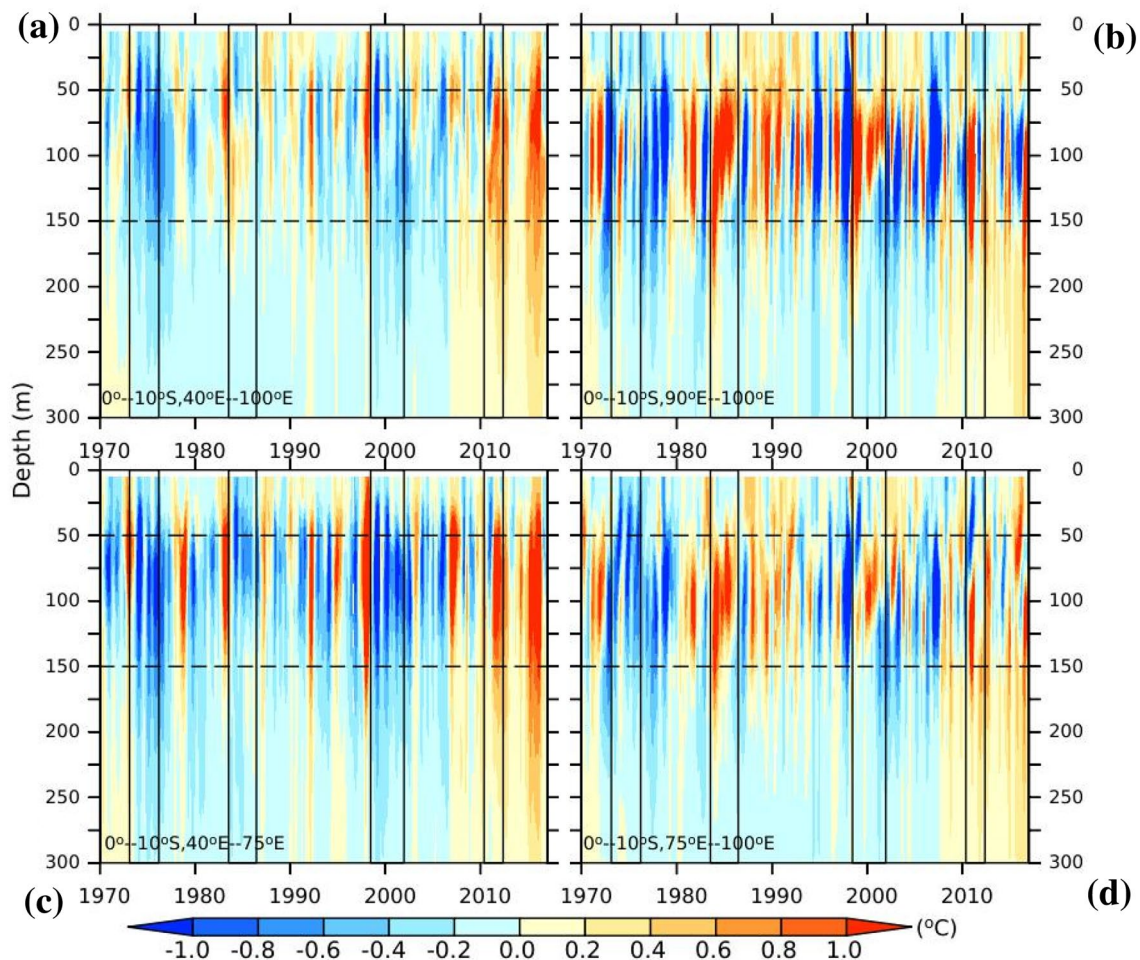


Fig. 1 Time depth section of spatially averaged temperature anomaly profiles averaged over different regions **a** 0°–10° S, 40° E–100° E, **b** 0°–10° S, 90° E–100° E, **c** 0°–10° S, 40° E–75° E and **d** 0°–10° S, 75° E–100° E. The abscissa represents the time and the ordinate represents

depth. The dashed horizontal black lines represent the 50 m and 150 m depth levels. The four black vertical line pairs represent the prolonged La Niña events

the equator (Fig. 2d, e). But during the 1973–1976 and 2010–2012 La Niña events, the cold tongue spreads over both north and south (Fig. 2c, f). These latitudinal spreads of the cold tongues are associated with the Pacific Decadal Oscillation (PDO) or IPO phases with more latitudinal spread during the cold phase of PDO. During 1973–1976 and 2010–2012 when the cold tongues of the La Niña spreads both sides of the equator, the PDO was in cold phase. Moreover, during the other two events when the cold tongue of La Niña is mostly confined near the equator, PDO phase was positive. Enhanced warming all along the western Pacific is seen only during the 1998–2001 La Niña event (Fig. 2e). Although enhanced warming is seen in the southwestern tropical Pacific during 1973–1976, 1998–2001 and 2010–2012 La Niña events, the warming in the northwestern Pacific is evident only during 1998–2001 (Fig. 2d). This enhancement in the warming over northwestern Pacific is closely associated with the strong anti-cyclonic surface

winds over the region (Fig. 2d) which effectively weakens the mean winds over the northwestern Pacific and reduces the evaporative cooling and promotes SST warming. During all these La Niña events, strong surface easterlies are seen in the western and central Pacific region. These easterlies are stronger during the cold PDO phase due to the stronger SST gradient formed with intense cooling over the central Pacific region and warming in the west. The easterly winds are strongest in the western Pacific during the 2010–2012 La Niña event compared to the other La Niña events.

During the prolonged La Niña events, most of the Indian Ocean displays cooling in the surface (Fig. 2) and is consistent with earlier studies (e.g., Singh et al. 2013; Chowdary et al. 2006). In all the events, weak warming over the southeastern TIO is apparent which is also part of a phenomena known as Ningaloo Niña off the west coast of Australia (Benthuisen et al. 2014; Zhang et al. 2018) (Fig. 2). During these prolonged La Niña periods, the winds over the

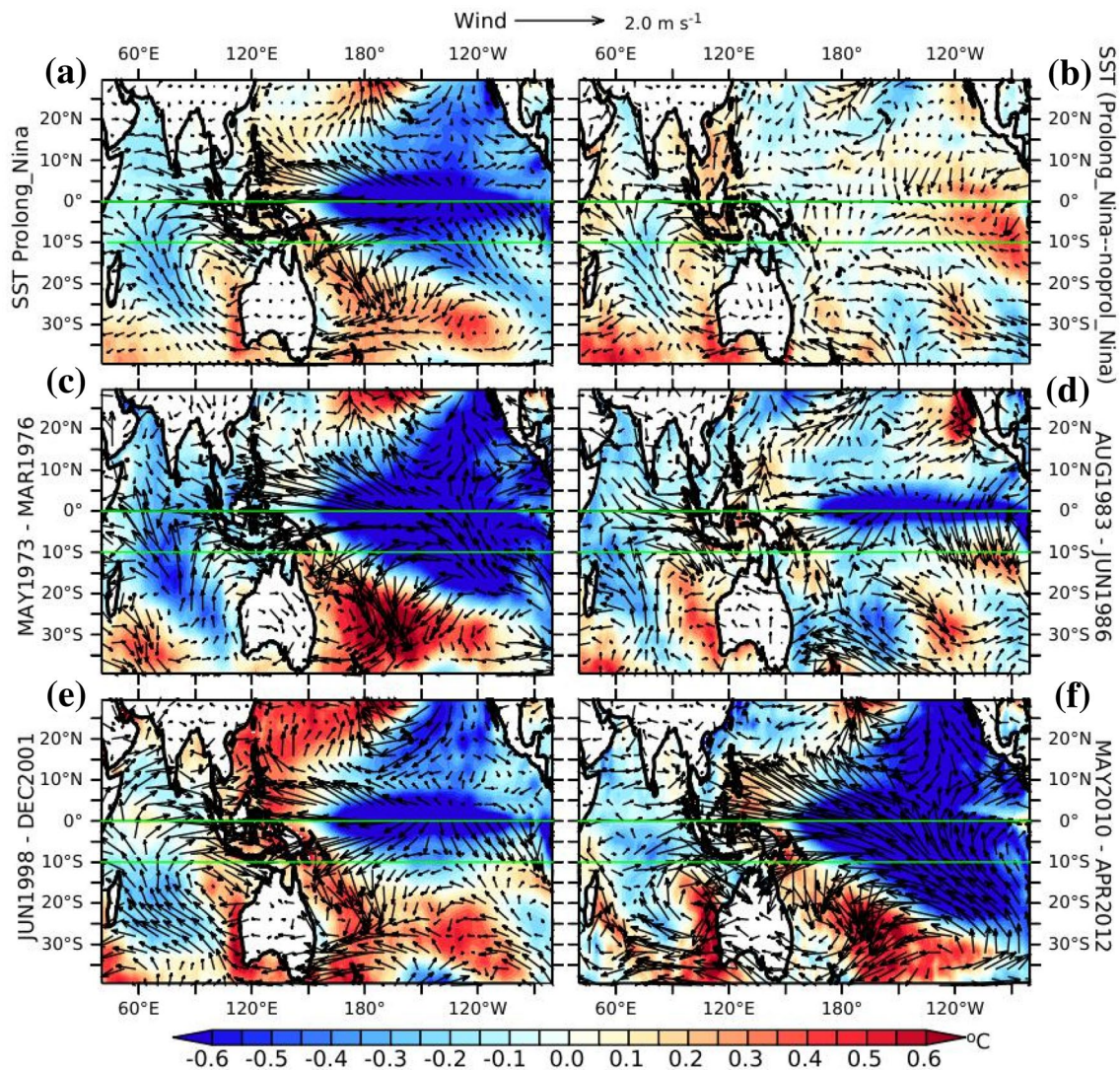


Fig. 2 SST anomaly ($^{\circ}\text{C}$, shaded) and surface (10 m) wind anomaly vectors (m s^{-1} , arrows) for the prolonged La Niña events. **a** Shows the composite for all the prolonged La Niña events. **b** Represents the difference between the composites of all the prolonged and non-pro-

longed La Niña events. **c–f** Shows the composites for the individual prolonged La Niña events of 1973–1976, 1983–1986, 1998–2001 and 2010–2012 respectively. Horizontal green lines represent the equator and 10°S latitude lines

EEIO are prominently westerlies. During 1973–1976 in the southeastern part of TIO warming is weak, whereas stronger cooling is seen in the southwestern part (Fig. 2b) of TIO. It is worth reporting the coherent evolution of EIO winds and TIO subsurface temperature with the Niño3.4 (Fig. 3). The time series of Niño3.4 index and the possible response of ENSO on the TIO in the form of EIO zonal winds, EEIO upper ocean temperature are shown in Fig. 3.

Previous studies reported that the interannual variability of the inter-basin exchanges such as ITF and winds over the TIO are closely associated with ENSO (e.g., Wijffels and Meyers 2004; Sprintall et al. 2009; Sprintall and Révelard 2014). The depth-time plot of area averaged temperature (Fig. 1) reveals that strong positive anomaly is apparent in

the 50–150 m depth level. Therefore, the top 150 m and 50–150 m averaged temperature over EEIO is compared with the Niño3.4 index to examine its relationship with the heat distribution (Fig. 3). It is important to note that the upper ocean (and subsurface) temperature over EEIO displays a clear out of phase relationship with the Niño3.4 index (Fig. 3). The variability in the 50–150 m temperature (Fig. 3) is consistent with Fig. 1. The temporal evolution of subsurface temperature reveals that prolonged La Niña events strongly influence the 50–150 m depth temperature (Fig. 3). The maximum intensity of the warming (cooling) in the eastern (western) parts is seen in the 50–150 m depth range (Fig. 1). The average winds along EIO during the prolonged La Niña events display strong and consistent

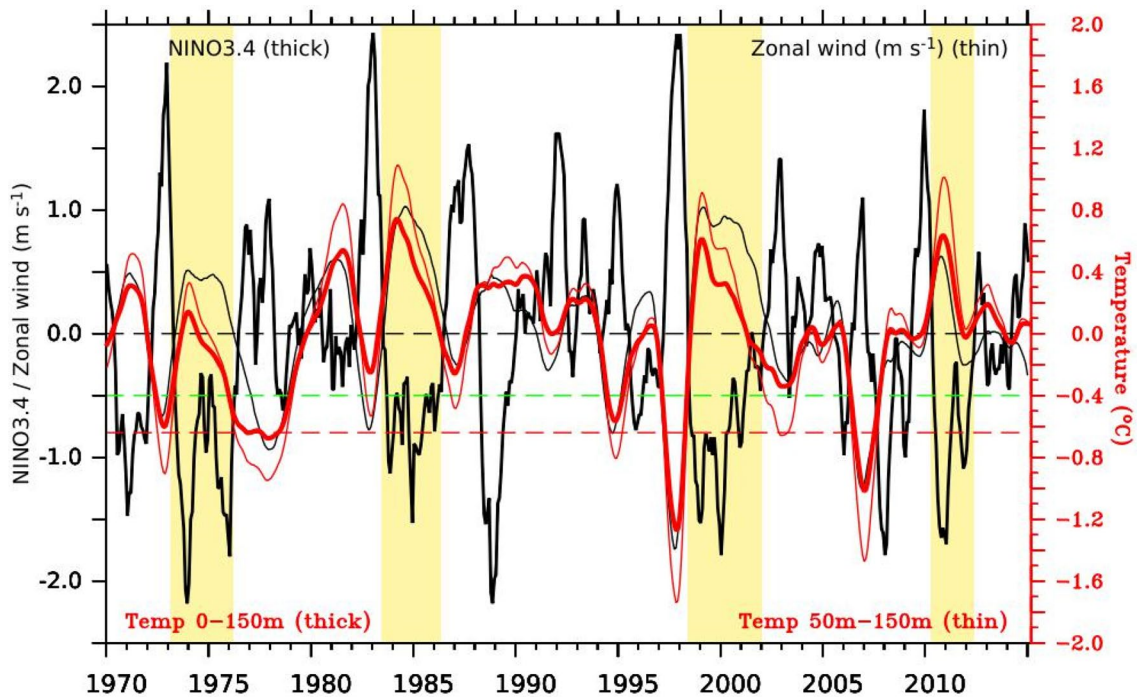


Fig. 3 3-month running mean of Niño3.4 index (thick black line), zonal wind anomaly (m s^{-1}) averaged over 60°E – 100°E , 5°S – 5°N (thin black line). The 25-month running means of top 150 m (50–150 m) average temperature over 90°E – 100°E , 5°S – 5°N region represents the thick (thin) red lines. The left axis represents the val-

ues of Niño3.4 index and zonal wind anomaly (m s^{-1}), and the right axis represents the temperature ($^{\circ}\text{C}$). The prolonged La Niña events of 1973–1976, 1983–1986, 1998–2001 and 2010–2012 are marked by beige shaded area. The dashed green line represents -0.5 SST anomaly and red dashed line represents 1 standard deviation (0.83)

westerlies over the eastern half of the EIO region (Fig. 3). Moreover, the 50–150 m temperature and the westerly wind anomaly follow similar variations (Fig. 3). These strong westerlies over EIO (Fig. 2) during the prolonged La Niña event, force downwelling Kelvin wave and Yoshida/Wyrtki Jet (Yoshida 1960; Wyrtki 1973; Luyten and Roemmich 1982; Clarke and Liu 1993; Hastenrath et al. 1993; Yamagata et al. 1996; Meyers 1996; Vinayachandran et al. 2009; Gnanaseelan et al. 2012). The downwelling Kelvin waves deepen the thermocline in the east, and on the other hand Yoshida/Wyrtki jet transports water from the west to east. Further, it is found that the EIO westerlies are influenced by the persistent La Niña forcing (Fig. 3). In addition to the eastern warming, there is intensified cooling over the western TIO during these prolonged La Niña events (Fig. 2).

In order to investigate the effect of the prolonged and non-prolonged La Niña events (westerlies) on TIO thermocline, the depth of 20°C isotherm (D20) composite is studied (Fig. 4). A deeper thermocline is evident along the eastern TIO in the prolonged La Niña composites especially for the northern and eastern part of BoB (Fig. 4c). In the similar way, the anomalous subsurface warming (rise in the 50–150 m heat content and temperature anomalies) and sea-level rise are also seen in the eastern TIO in the composites (Fig. 5). Also, anomalous shoaling of TRIO

(5°S – 15°S , 60°E – 90°E) thermocline, anomalous sea-level and heat-content low are seen with eastward extension during the prolonged La Niña events (Figs. 4a, c, e; 5c, d, e, f). Overall, remarkable difference in the eastward extension of TRIO region is evident from the thermocline, heat-content and sea-level anomalies during the prolonged La Niña events (Fig. 4a; 5a, b). The eastward extension of TRIO is closely associated with the wind patterns in the southeast TIO, which will be discussed later in Sect. 4. So, a thermocline deepening in the BoB and an eastward extension of the TRIO region and stronger westerlies in the eastern EIO are typical signatures associated with the prolonged La Niña events. Transport plays a crucial role in redistributing heat, so the spatial patterns of UOHC anomaly and transport over 50–150 m are examined. Warming (positive UOHC anomaly) is seen in the eastern parts of the TIO for each La Niña event and their composite (Fig. 6). The eastern warming is evident in the difference between the composites of prolonged and non-prolonged La Niña events as well (Fig. 6b). This indicates more intense warming in the 50–150 m depth levels for the prolonged La Niña events. Intense warming is however confined to the eastern TIO (including southeastern and eastern TIO and BoB) during the 1983–1986, 1998–2001 and 2010–2012 La Niña events (Fig. 6). Only during

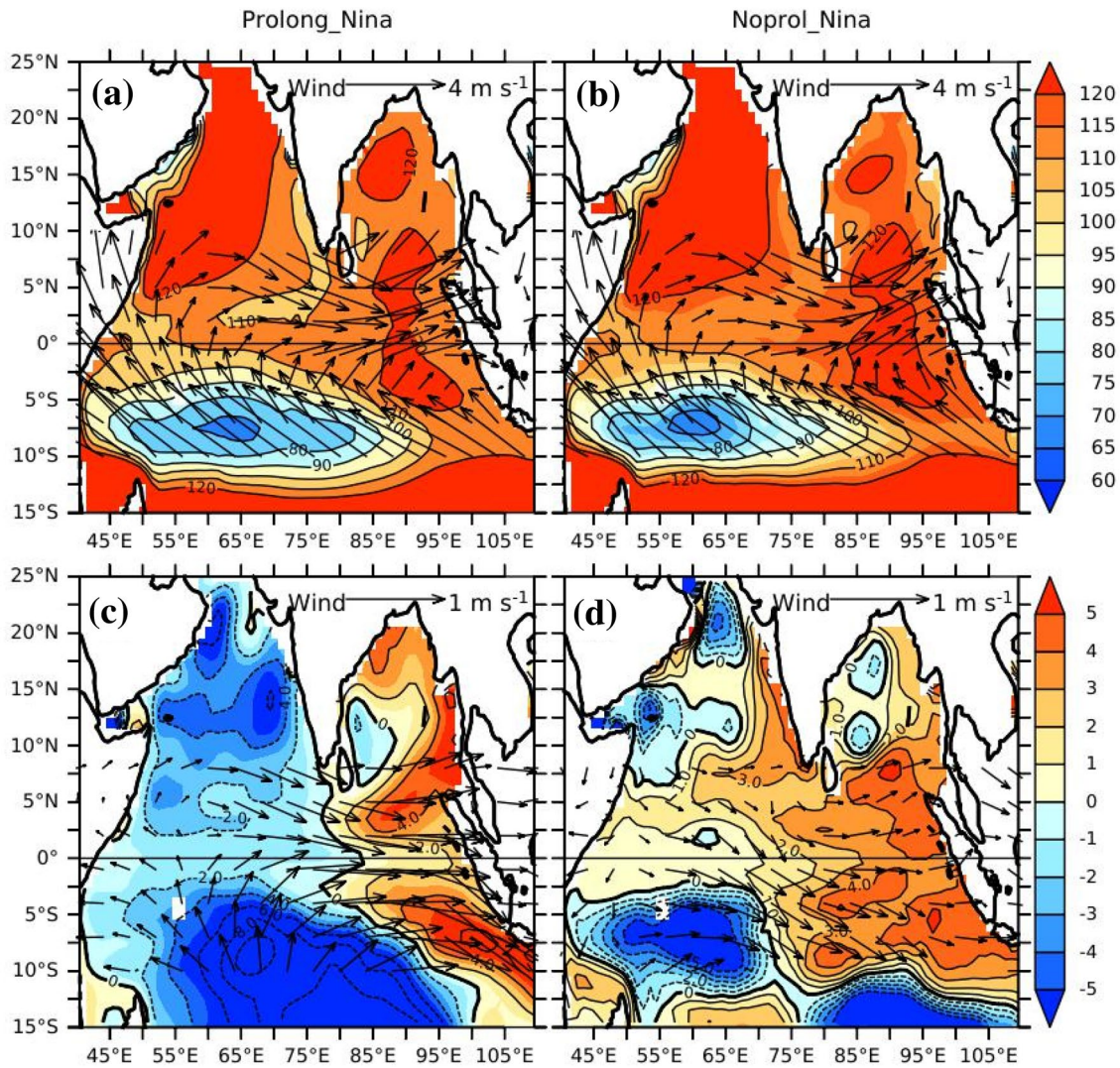


Fig. 4 The composites of the absolute values of D20 (m, shaded) and wind (m/s, vectors) for all the prolonged La Niña events of 1973–1976, 1983–1986, 1998–2001 and 2010–2012 is given in frame (a). **b** Is same as (a) but for all non-prolonged La Niña events. Frame **c**

represents the D20 and wind vectors same as frame **a** but for the composite of anomaly. Frame **d** represents the same as **b** but for the composites of anomaly

2010–2012, the warming is seen in the western parts also and is related to the anomalous positive wind stress curl over TRIO region from mid-2011 onwards (i.e. the later phase of the prolonged La Niña event) and the associated downwelling (Fig. 6f). The warming during 1973–1976 is weak and confined mostly to the eastern boundary with an intense cooling in the TRIO region (Fig. 6b). The warming in the BoB is confined to the eastern boundary and most part of the northern region north of 15°N including northwestern boundary of BoB (Fig. 6), which is also evident in the positive sea-level anomaly (figure not shown). This is an indication of downwelling coastal Kelvin waves forced by the equatorial westerlies (Figs. 2 and 3). Moreover, downwelling Rossby waves radiated from the eastern boundary propagate westward, redistributing heat towards

the interior BoB. The warming is more intense in the winter (November through February, NDJF) and spring (March through May, MAM) seasons. Due to the presence of an intense cooling during the summer monsoon (June through September, JJAS) season, 1973–1976 La Niña event witnessed weaker warming (figure not shown). The prolonged La Niña witnessed intense cooling in the southwestern part including TRIO region (Fig. 6) and the maximum cooling is seen during 1998–2001 La Niña whereas weaker cooling is observed during 1983–1986 (Fig. 6e, d). This cooling extends eastward for the prolonged La Niña event and is also seen in the difference between the composites of prolonged and non-prolonged La Niña events (Fig. 6b) and is consistent with the sea-level anomaly composite as well (Fig. 5b).

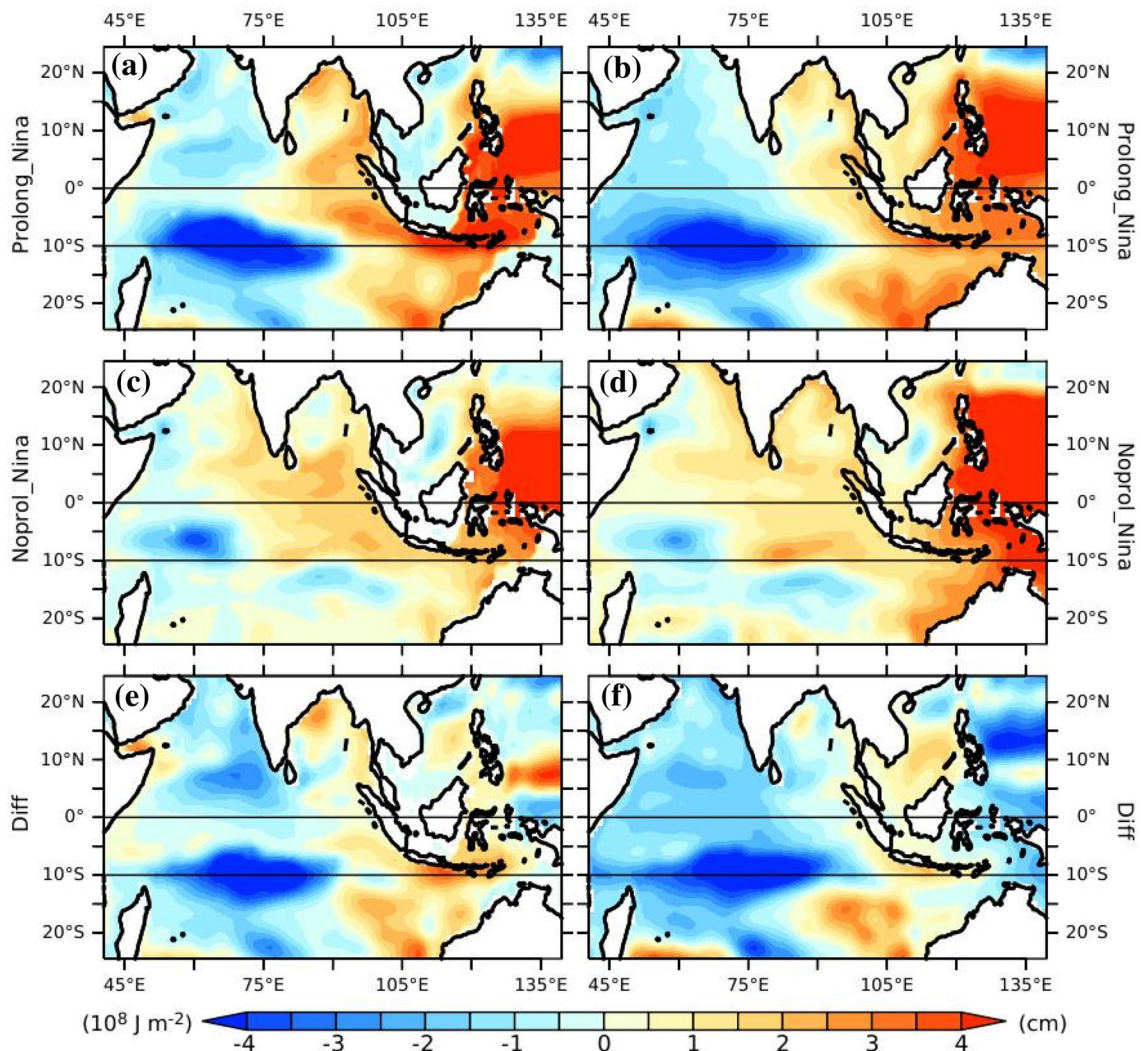


Fig. 5 The composites of heat content (10^8 J m^{-2}) for 50–150 m (left panels; a, c, e) and sea-level-anomaly (cm) (right panels; b, d, f) for prolonged La Niña events (a, b), non-prolonged La Niña events (c, d)

and difference of the composites of the prolonged and non-prolonged La Niña events (e, f). The black lines represent the equator and 10° S latitude in each panel

4 Volume transport in the 50–150 m level

The Rossby wave propagating from the Pacific contributes to the interannual variability in the southern TIO (e.g. Vaid et al. 2007). It is noted by Rahul and Gnanaseelan (2016) and Deepa et al. (2019) that the waves propagating from the Pacific Ocean to the TIO through ITF contribute to the sea level variations in the eastern TIO. In this study, it is found that the warming (seen in the heat content) in the eastern side of TIO is present mainly during the prolonged La Niña events when a cyclonic wind circulation is prevailing mainly over the southeastern TIO (Figs. 2, 7). This cyclonic circulation pattern in the southeastern TIO is a unique feature of the prolonged La Niña events (Figs. 2, 7). It is clearly visible in the composite of rotational wind anomaly of all the prolonged La Niña events

and also the difference between the prolonged and non-prolonged La Niña events (Figs. 7a,b).

The negative wind stress curl due to the cyclonic wind (Fig. 7) forces upwelling Rossby waves that propagate westward (Fig. 8) and contribute to the cooling around the TRIO region (Fig. 6a). The negative wind stress curl shoals the thermocline as well, extending the cooling eastward, thereby extending the TRIO region eastward (Fig. 4d). These patterns persist for the entire period and enhance cooling and shoal the thermocline in the TRIO region (Figs. 4, 5, 6). However, in the eastern EIO the winds are westerlies during the La Niña period and consequently east of 90° E edge of this wind pattern exhibits strong positive wind stress curl as well as eastward propagating Kelvin wave and Yoshida/Wyrtki jet (as discussed in Sect. 3) along the eastern boundary of southeastern TIO (Fig. 7). The eastward propagating

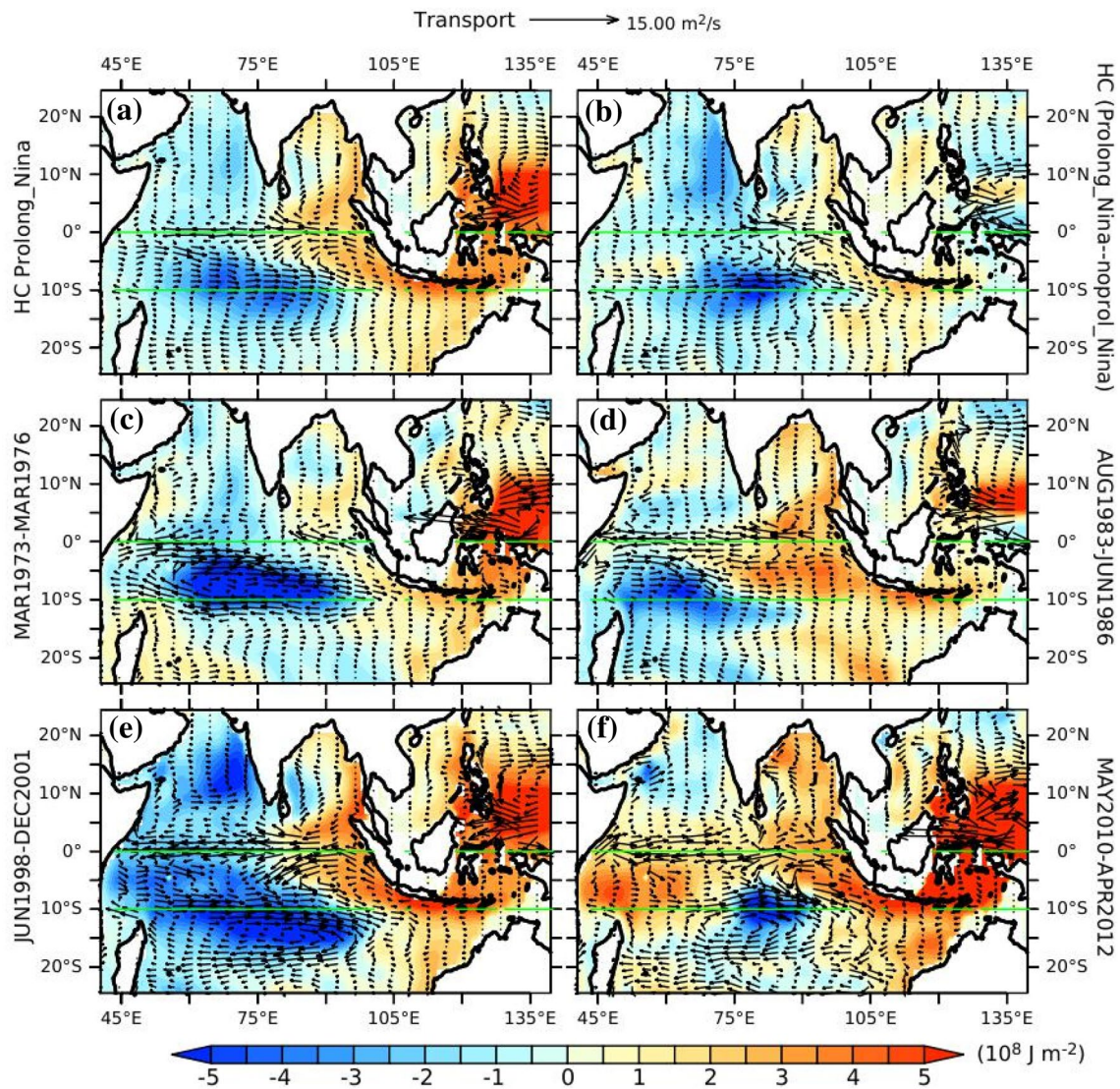


Fig. 6 Spatial pattern of average heat content anomaly (10^8 J m^{-2} , shaded) and volume transport (vectors, $\text{m}^2 \text{ s}^{-1}$) integrated over the 50–150 m depth level calculated from the ORAS4 data. **a** Represents the composite for all the prolonged La Niña events, **b** represents differences between composites of all prolonged and non-prolonged La

Niña events. **c–f** Show the composites for the individual prolonged La Niña events of 1973–1976, 1983–1986, 1998–2001 and 2010–2012 respectively. Horizontal green lines represent the equator and 10° S latitude lines

downwelling Kelvin wave and Yoshida/Wyrtki jet promote warming in the eastern EIO (Fig. 9) and deepens the thermocline near the eastern boundary (Fig. 4).

The time longitude (Hovmöller) diagram (of 50–150 m heat-content anomalies and sea level anomalies averaged over 5° S – 12° S) shows the Rossby wave propagation and the associated UOHC anomaly during the prolonged La Niña events (Fig. 8). The cooling (warming) in this region is associated with the negative (positive) sea-level anomaly (SLA). As the propagation of the upwelling Rossby wave is associated with the cooling, which is evident in the co-propagation of heat content anomaly and SLA. Therefore, the cooling process is triggered by these Rossby waves. It

is also important to note that the upwelling Rossby waves shoal the thermocline in the TRIO region. The associated upwelling is responsible for the cooling observed during the prolonged La Niña events.

The depth longitude cross sections of zonal and vertical currents and temperature anomalies averaged in the eastern TIO show downward currents and subsurface warming (Fig. 9a–e) and cooling in the western or central region (within 0–150 m depth), with maximum temperature anomaly between 50 and 150 m (Fig. 9). A stronger warming and eastward zonal current in the southeastern TIO is evident during the prolonged La Niña events compared to non-prolonged La Niña (Fig. 9b). In spite of the downwelling at the

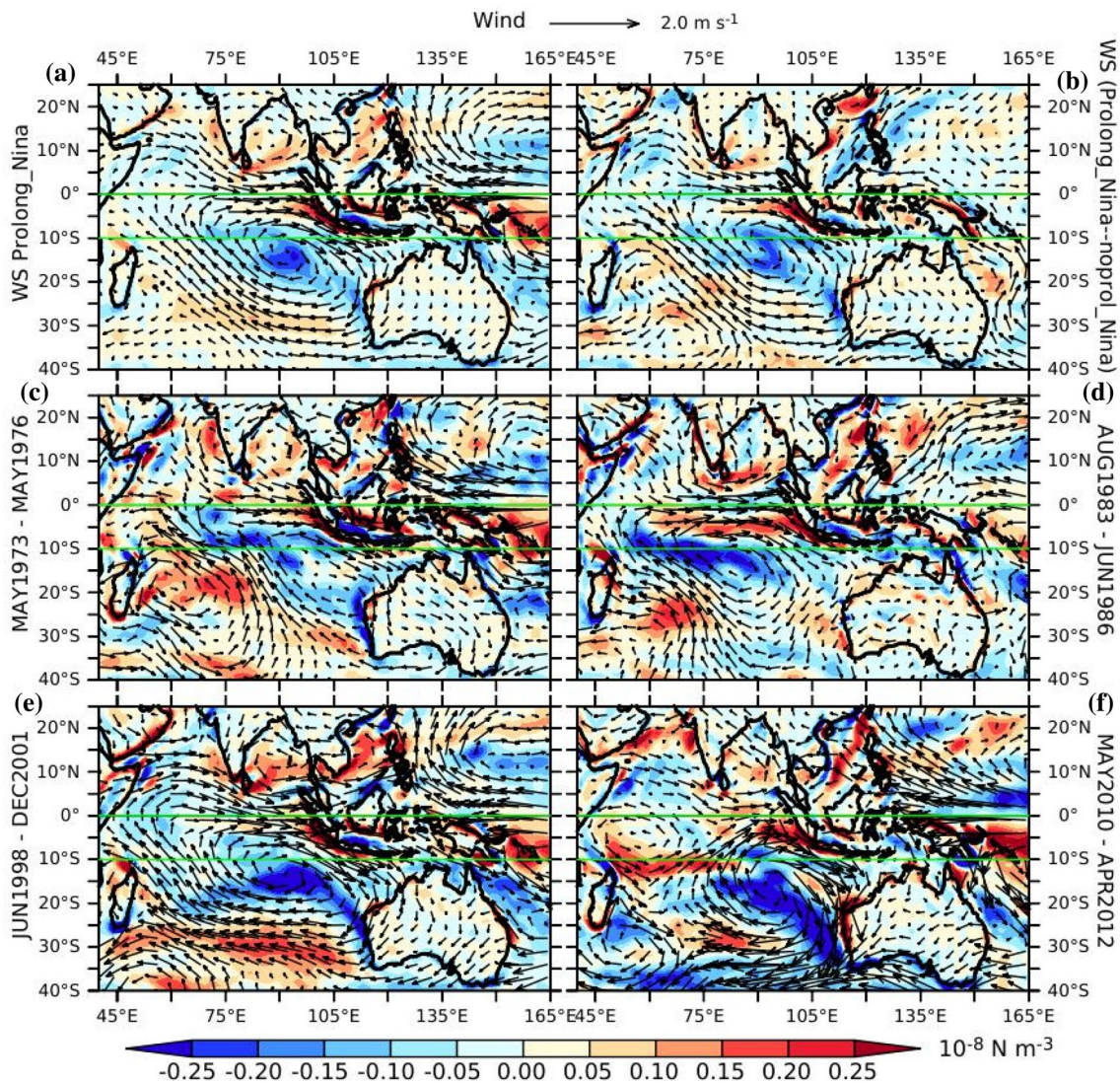


Fig. 7 Anomalous wind stress curl (shaded, N m^{-3}) and rotational wind anomaly (vector, m s^{-1}) composites from ERA data. **a** Represents composites for all the prolonged La Niña events, **b** represents differences between composites of all prolonged and non-prolonged

La Niña events. **c–f** represents composites for individual prolonged La Niña events of 1973–1976, 1983–1986, 1998–2001 and 2010–2012 respectively. Horizontal green lines represent the equator and 10°S latitude lines

eastern boundary, the advection of colder water from the western EIO weakens the intensity of the warming in the EEIO region (Fig. 10).

The anomalous warm water advection from the western Pacific is also evident during the prolonged La Niña events (Fig. 10). Figure 11 shows the meridional Sverdrup transport at the equator and the equatorial belt of 5°S – 5°N . The entire longitudinal extent and only the eastern region are shown to understand the relative contribution from the east. The cross-equatorial Sverdrup transport is found significant along the eastern part of the EIO during the prolonged La Niña events (Fig. 11). This supports the existence of cross-equatorial oceanic heat transport near the EEIO region through Sverdrup transport. The origin of this warm water

is from western Pacific through ITF to the southeastern TIO (Fig. 10). As the transport from the western EIO is not contributing to the warming in the east (Fig. 9), the warming observed in the eastern EIO and BoB are contributed by the cross-equatorial Sverdrup transport (Fig. 10). This suggests the possible pathway for the warm western Pacific waters entering in the northeastern EIO and BoB.

Further, the temporal variability of the 50–150 m heat content and sea-level anomaly in the eastern (5°S – 5°N , 80°E – 105°E), southeastern TIO (15°S – 5°S , 100°E – 120°E), part of BoB (5°N – 20°N , 80°E – 100°E) and TRIO (15°S – 5°S , 60°E – 90°E) regions are studied. To extract interannual variability the 2–7-year band-pass filtered signals are considered. The co-evolution of anomalous

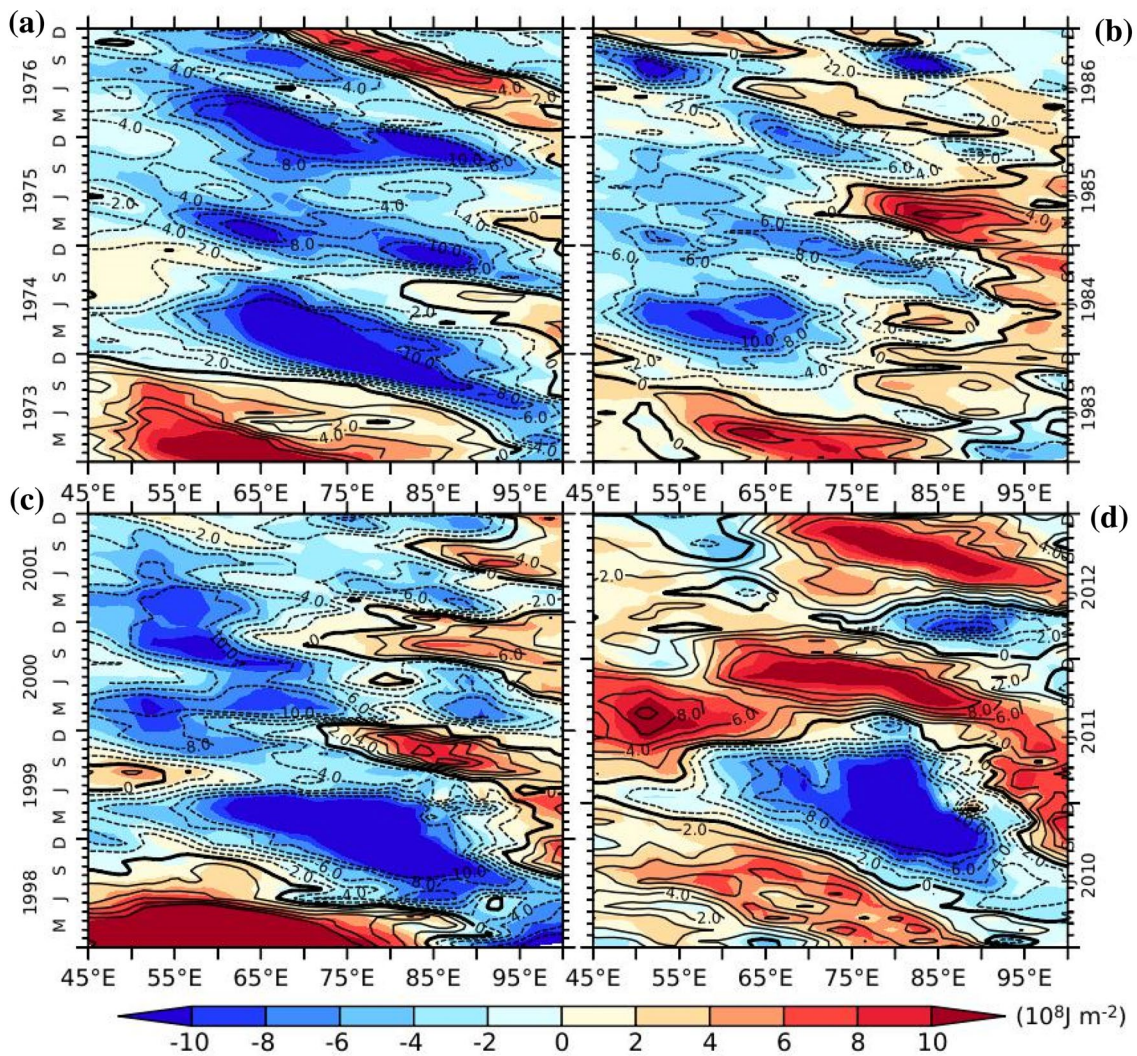


Fig. 8 Hovmöller diagram (longitude vs. time) for heat content anomaly (HCA) for 50–150 m depth level along with sea-level-anomaly (SLA) averaged over 5° S–12° S during the prolonged La Niña events. The shaded colours represents the HCA (10^8 J m^{-2}) and the

contours represents SLA (cm). **a–d** Represents the HCA and SLA for prolonged La Niña events of 1973–1976, 1983–1986, 1998–2001, and 2010–2012 respectively. Both HCA and SLA are derived from the ORAS4 data

features in all the regions suggests the strong impact of prolonged La Niña forcing through common mechanisms such as equatorial westerlies. The time series of heat content shows warming (positive anomaly) in the eastern TIO during the prolonged La Niña events similar to the spatial patterns (Figs. 6, 12). This intense cooling in the TRIO region during the prolonged La Niña events are seen in the time series (Fig. 12d). The sea-level anomaly mimics the heat content pattern very closely (Figs. 12, 13). Figures 12 and 13 show the existence of strong inter-annual variability for both the UOHC and sea-level anomaly over these regions. It is evident that during these La Niña events the inter-annual variability (shown by the green curve in Figs. 12a–c, and 13a–c) is dominant (with respect to the magnitude in the time series shown by the red curve in Figs. 12a–c, 13a–c).

As TIO shows strong seasonality, it is important to understand heat distribution patterns in the different seasons of these prolonged La Niña events. Our analysis with the spatial plots for the different seasons confirms the intense warming during the winter (November through February, NDJF) and spring (March through May, MAM) seasons. Each prolonged La Niña event is characterized by strong warming (cooling) in the eastern part (TRIO region) of the TIO for the entire La Niña period (Fig. 14). Hence, the role of seasonality is less significant for this phenomenon compared to the inter-annual variability.

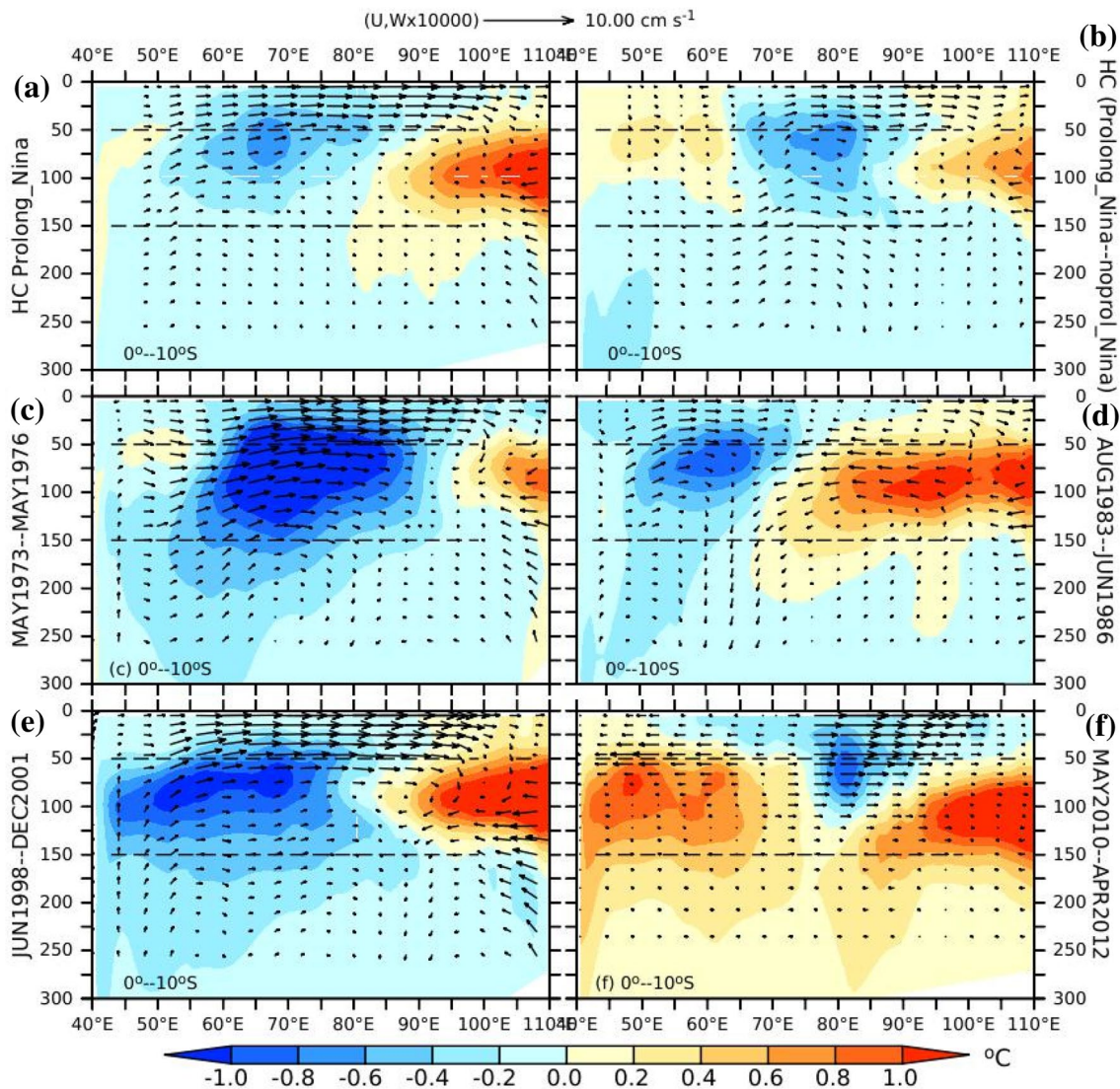


Fig. 9 Depth longitude section temperature anomaly ($^{\circ}\text{C}$) profiles averaged over the prolonged La Niña events within the latitude range of 0° – 10° S. The vectors represent the zonal vs. vertical ($\times 10^4$) current (cm s^{-1}) averaged over the same spatial and temporal spans as the temperature profiles. **a** Represents the composite of temperature and current vector for all the prolonged La Niña events. **b** Represents the difference between composites of prolonged and non-prolonged La Niña events for the same. **c–f** Represents the temperature and cur-

rent vector composites for the individual prolonged La Niña events of 1973–1976, 1983–1986, 1998–2001, 2010–2012 respectively. In all the frames the zonal velocity is taken from ORAS4 data but the vertical currents are taken from the ORAS3 data. In frame **d** the vertical currents are kept as zero for the 2010–2012 La Niña event as they are not available beyond 2009 in the ORAS3 data set. For the same reason the first three prolonged La Niña events represented in **b**, **c** and **d** are taken into account while taking the composite for frame **(a)**

5 Summary and discussion

In this paper the heat distribution in the TIO is examined during the prolonged La Niña events. We have considered the recent four prolonged La Niña events (1973–1976, 1983–1986, 1998–2001 and 2010–2012) as case studies in addition to the composite analysis. It is found that prolonged La Niña events induce basin-wide surface cooling in TIO (Fig. 2). In addition to the basin wide surface cooling, sub-surface cooling in the southwestern and subsurface warming

in the southeastern TIO are seen (Fig. 6). Anomalous negative wind stress curl associated with the cyclonic wind pattern over the southeastern TIO is found to be the unique feature of a prolonged La Niña event (Fig. 7). The upwelling Rossby wave forced by the cyclonic winds in the southeastern TIO propagates westward and contributes to the intense cooling over TRIO region and the western TIO (Figs. 6, 8). The anomalous transport of warm ITF water from the western Pacific helps to warm the southeastern TIO (Fig. 10). In contrast, along the equator, anomalous zonal advection

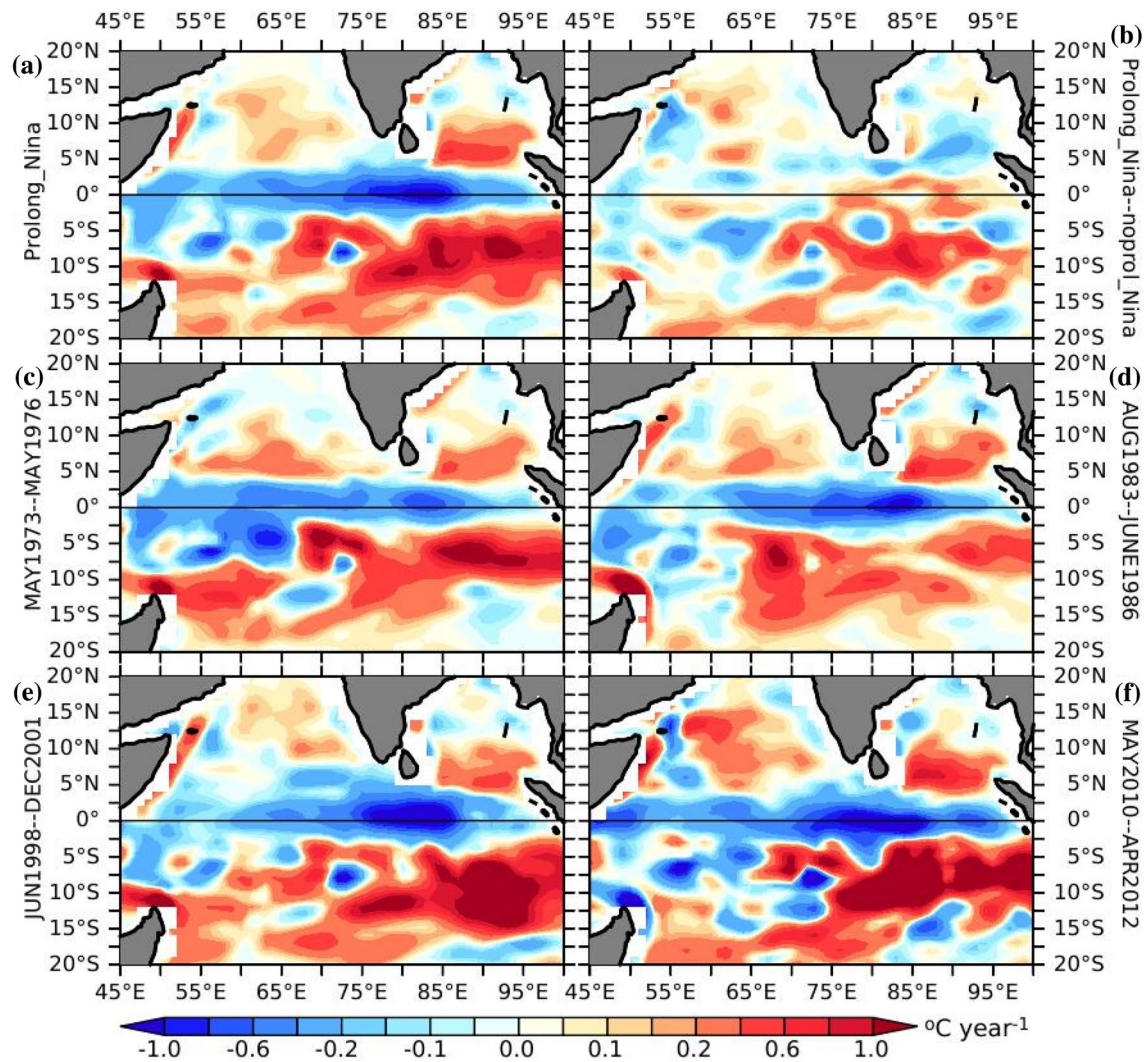


Fig. 10 The zonal advective heat flux component ($^{\circ}\text{C year}^{-1}$), of the heat budget for 50–150 m depth level for the prolonged La Niña events. **a** Represents the composite of all the prolonged La Niña events. **b** Represents the difference of the composites for the pro-

longed and non-prolonged La Niña events. **c–f** Denote the zonal advection term for the individual prolonged La Niña event of 1973–1976, 1983–1986, 1998–2001, 2010–2012 respectively. The horizontal black line represents the equator

brings cold water from the western EIO and reduces the intensity of the warming in the eastern EIO at 50–150 m during the prolonged La Niña events (Figs. 3, 9, 10). The cross equatorial Sverdrup transport during the prolonged La Niña events shows northward cross-equatorial flow in the eastern TIO region, which is important in warming the northeastern TIO or BoB (Fig. 11). The cross equatorial meridional Sverdrup transport is found to transport the ITF water to the northeastern TIO (BoB). The warming along the eastern parts of TIO, thermocline deepening (Fig. 4), northward cross-equatorial flow along the eastern boundary (Fig. 11), intense cooling at the western TIO especially in the TRIO region (Fig. 6), its eastward expansion are the typical characteristic features associated with the prolonged La Niña events (Figs. 4, 5). Analysis reveals that the warming

is not confined to the EEIO but extended all the way up to the head BoB with a significant thermocline deepening there (Figs. 4, 6). Most of the eastern TIO warming and western cooling are restricted within the 50–150 m levels during the prolonged La Niña events (Fig. 1). Also, downwelling Kelvin waves forced by the stronger westerlies induce downwelling and deepening of the thermocline at the eastern region (Figs. 4, 7, 9).

Further, time series analysis of 50–150 m heat content and sea-level shows that the inter-annual variability dominates the eastern TIO during these prolonged La Niña events. It is found that the seasonality of the TIO is of less significance compared to the interannual variability, though the warming (cooling) along the eastern TIO (TRIO) region are little more intense in winter (NDJF) and spring (MAM)

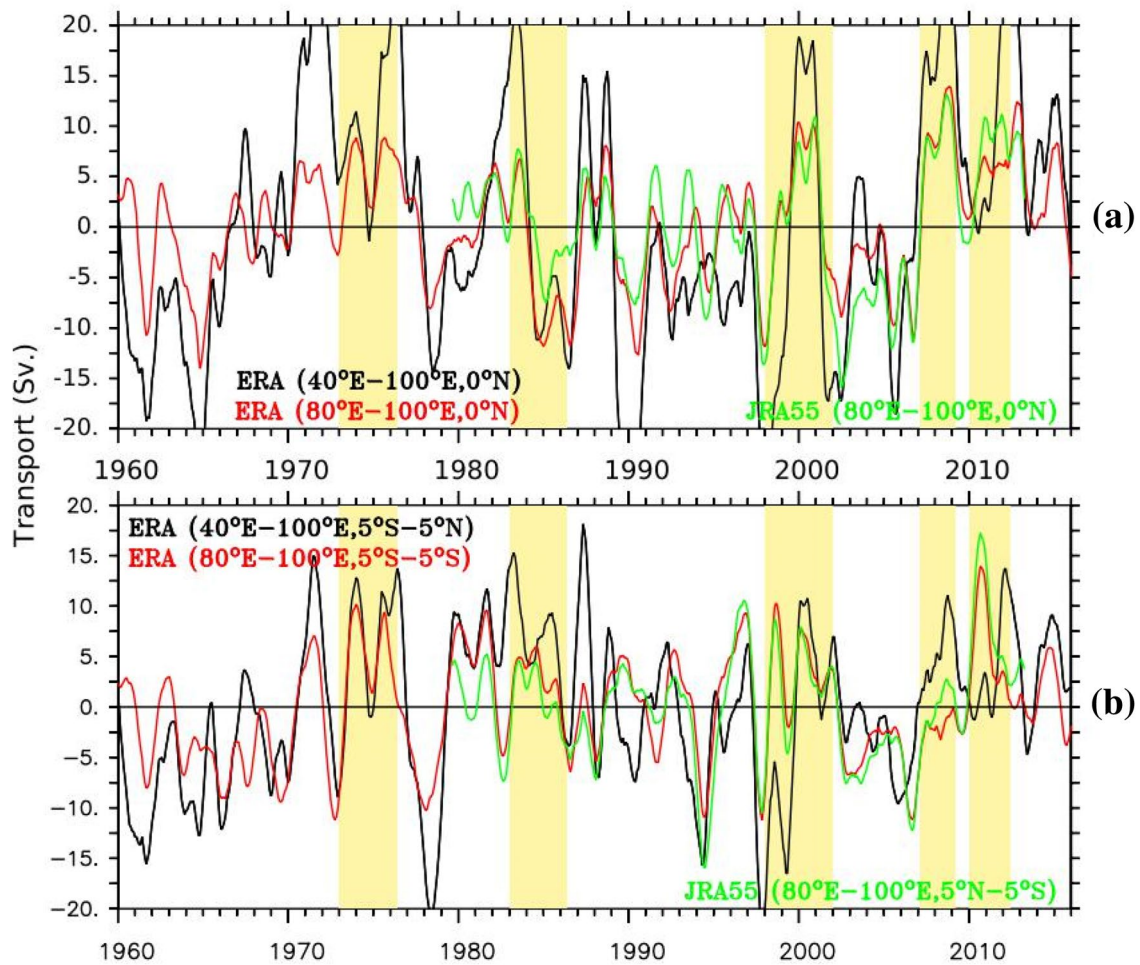


Fig. 11 Meridional Sverdrup transport (Sv) calculated from zonal wind stress during 1960–2017. **a** Represents the meridional cross-equatorial transport at the equator. **b** Represents the same averaged

over 5°S – 5°N . The black and red curve in each panel represents the Sverdrup transport calculated from ERA data and the green curve represents the same calculated from JRA55 data

during the prolonged La Niña events compared to the other seasons. Moreover, it is found that the warming along the eastern TIO is greatly controlled by the La Niña and IOD. East–west gradient in SST and heat content in the TIO during the prolonged La Niña events may strongly influence the local air sea interaction, mean state and the regional climatic conditions. This study is important in the context of possible pathways of heat entering the north Indian Ocean from Pacific during the recent global hiatus period since the mean state of Pacific resembled that of the La Niña during this period.

It is also worth noting that during the 1988–1989 event, which is strong but short lived La Niña, the typical anomalous cooling over the western TIO is not seen. In the case of 2007–2009 La Niña event, the anomalous cooling is seen in the eastern TIO in the second half. This cooling is related to the successive occurrence of positive Indian Ocean Dipole (IOD) events during 2006, 2007 and 2008. The associated

equatorial winds are easterlies during this period (Fig. 3). This suggests the possible role of local forcing (within the basin) in modulating the influence of La Niña impact (both warming or cooling over the TIO region).

It is seen that when La Niña and negative IOD (El Niño and positive IOD) conditions co-occur, they contribute to the enhanced warming (cooling) and sea-level rise (fall) in the eastern TIO. The enhanced warming events over the eastern TIO are reported during 1974, 1996, 1998, and 2010 when La Niña co-occurs with the negative IOD events. All these strong negative IOD events co-occurred with strong La Niña events resulting enhanced eastern warming (w.r.t. heat content) and sea-level rise (Figs. 12a–c; 13a–c). In contrast, enhanced cooling and negative sea-level anomaly is seen in the TRIO region (Figs. 12d, 13d). During 1974, 1998, 2010 the sea-level anomaly in the TRIO region reduces up to 12–15 cm (Fig. 13d). Maximum anomalies are observed during the prolonged La Niña events. It is worth noting that

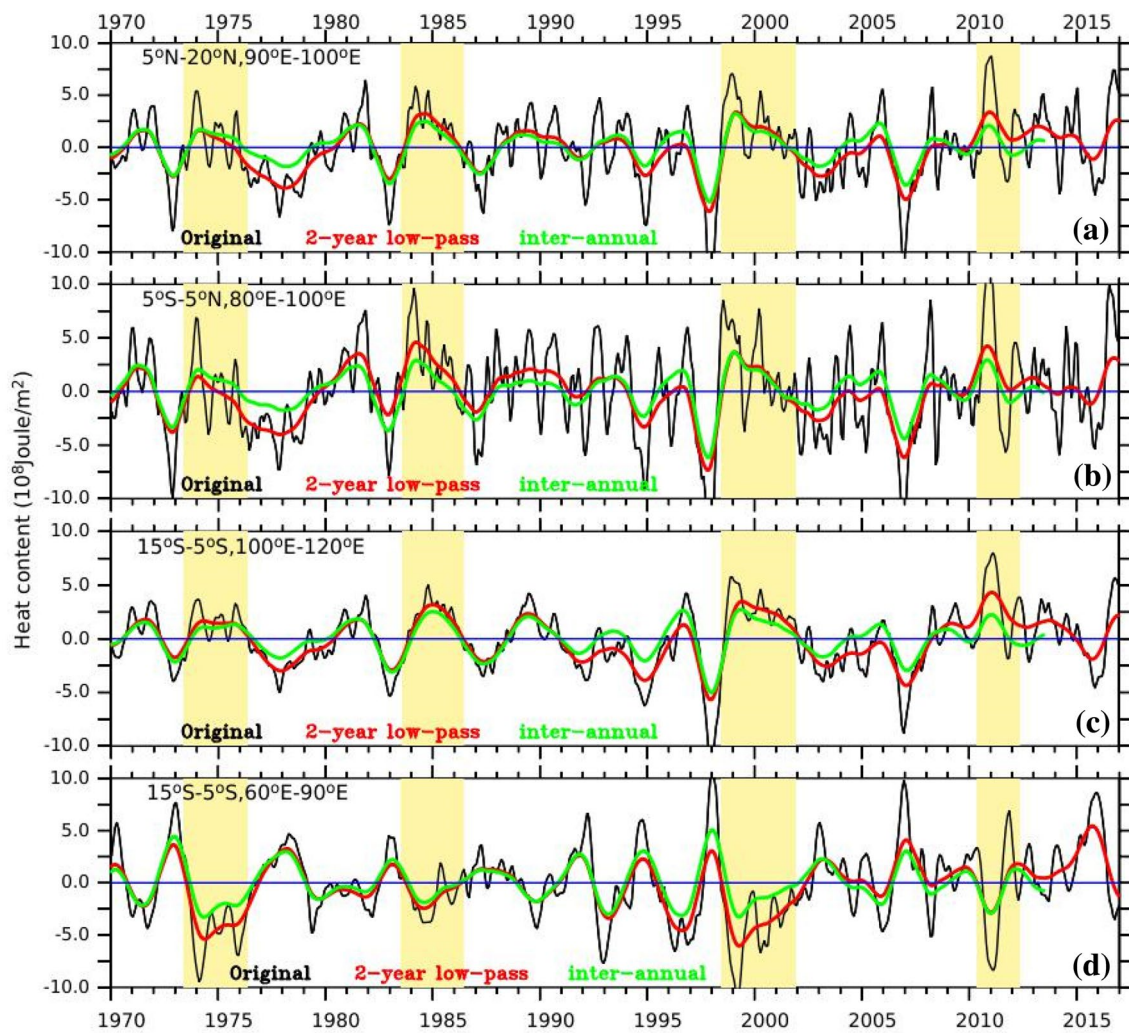


Fig. 12 Time series of UOHC anomaly integrated over 50–150 m depth range during 1970–2016. The frame **a** represents the UOHC averaged over the region 5° N–20° N, 90° E–100° E. Likewise frame **b–d** represents the same averaged over the regions 5° S–5° N, 80° E–100° E; 5° S–15° S, 100° E–120° E; 5° S–15° S, 60° E–90° E

(TRIO region). In each panel black curve represents 3-month running mean and red curve represents 25-month running mean. The green curve in each panel represents the inter-annual (2–7 year periodicity) component. The beige shaded area represents the prolonged La Niña events chosen for the study

during the moderate La Niña year 1996, which co-occurred with negative IOD supported the enhanced warming, however the amplitude is less than that of the prolonged La Niña events (Fig. 12).

The recent studies have shown that the heat transport from the Pacific Ocean to Indian Ocean is not only confined to the southern TIO but also influences the NIO (Nieves et al. 2015; Cheng et al. 2015; Ma et al. 2019). Moreover, the heat storage in the subsurface layers, especially in the thermocline, over a long period of time (typically a few years) may have cumulative impact on the sea level, and SST anomalies compared to that of shorter period. Such influences on the BoB are of prime importance, mainly due to

their potential influence on the cyclone activity, convection, and monsoon rainfall. In general, ENSO is known to have strong impact on Indian Ocean climate (Klein et al. 1999; Schott et al. 2009; Wu et al. 2010; Xie et al. 2016; Chen et al. 2017, 2019; He et al. 2020). Compared to the conventional ENSO the prolonged ENSO have stronger impacts on the TIO SST and heat content variability as evidenced in our study. In particular, many La Niña events persisted for more than 24 months. These prolonged La Niña events modulate the upper ocean heat distribution and sea-level over TIO to a greater extent. Intense cooling and anomalous sea-level low across the TRIO and the Arabian Sea is also found during the prolonged La Niña events.

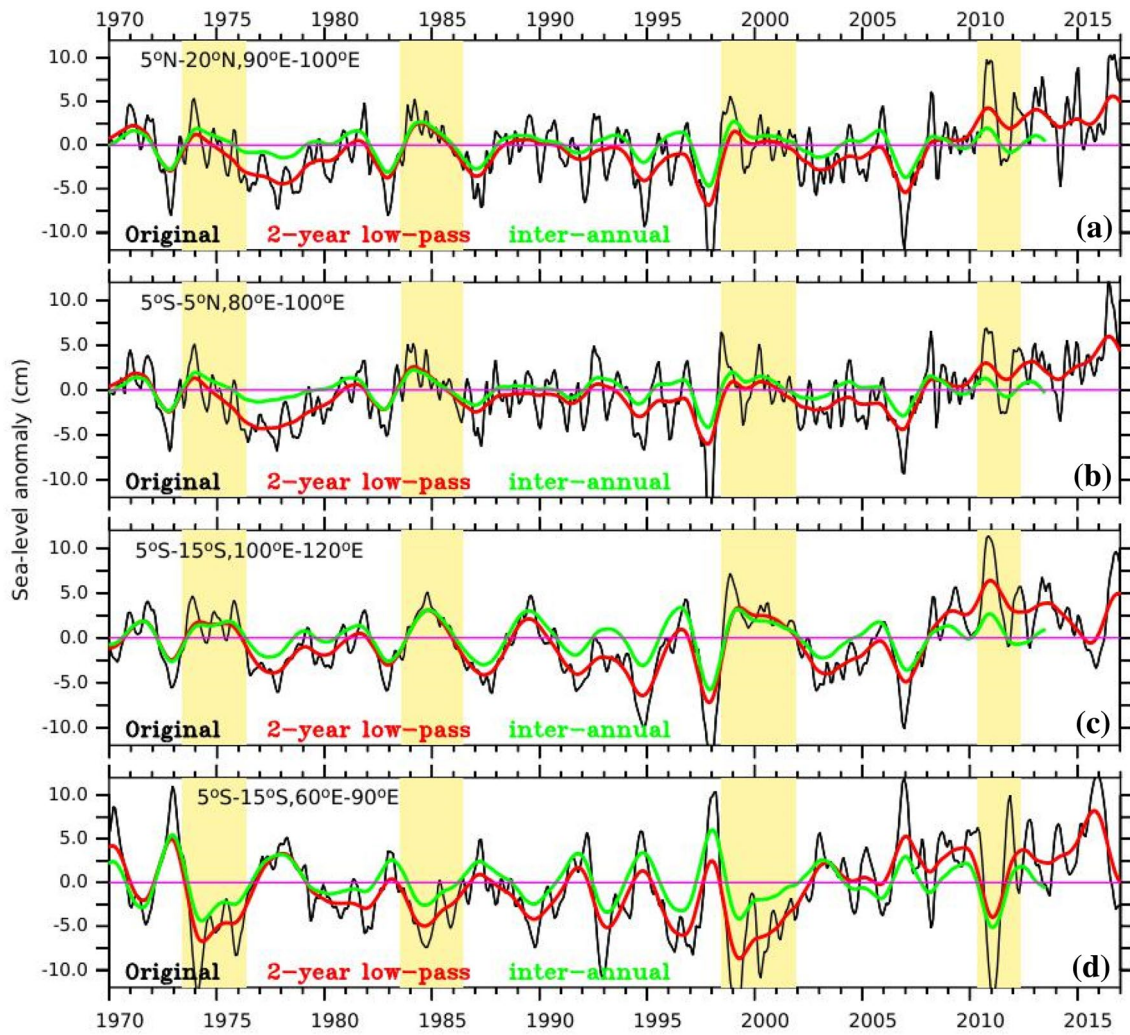


Fig. 13 Time series of sea-level anomaly (cm) during 1970–2016. The frame **a** represents the sea-level averaged over the region 5° N–20° N, 90° E–100° E. Likewise frame **b–d** represents the same averaged over the region 5° S–5° N, 80° E–100° E; 5° S–15° S, 100° E–120° E; 5° S–15° S, 60° E–90° E (TRIO region). In each

panel black curve represents 3-month running mean and red curve represents 25-month running mean. The green curve in each panel represents the inter-annual (2–7 year periodicity) component. The beige shaded area represents the prolonged La Niña events chosen for the study

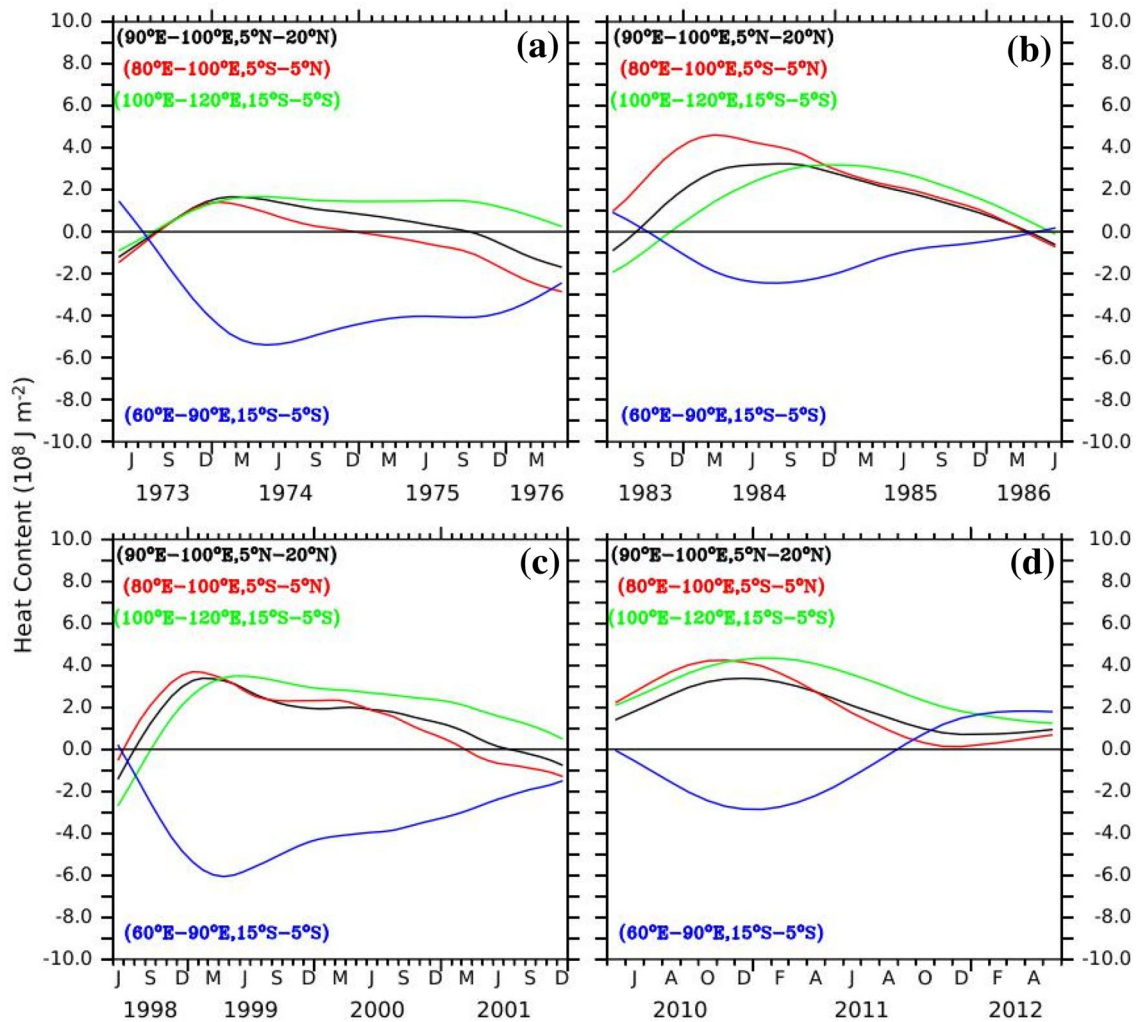


Fig. 14 Time series of average UOHC anomaly integrated over the 50–150 m depth level for the prolonged La Niña events of 1973–1976, 1983–1986, 1998–2001 and 2010–2012. **a–d** Shows the time series for 1973–1976, 1983–1986, 1998–2001 and 2010–2012.

Acknowledgements We thank Director, IITM, and Ministry of Earth Sciences (MoES), Government of India for support. The authors thank the various data centers for making the datasets available. ORAS4 sea level and temperature data are obtained from APDRC (<http://apdrc.soest.hawaii.edu/data/data.php>). PyFerret has been used for analysis and graphics. We thank the three anonymous reviewers for their valuable comments and suggestions.

References

Alexander MA, Blade I, Newman M, Lanzante JR, Lau NC, Scott JD (2002) The atmospheric bridge: The influence of enso teleconnections on air–sea interaction over the global oceans. *J Clim* 15(16):2205–2231. [https://doi.org/10.1175/1520-0442\(2002\)015<2205:TABTIO.2.0.CO;2](https://doi.org/10.1175/1520-0442(2002)015<2205:TABTIO.2.0.CO;2)

The black curve represents the UOHC anomaly for the 5° N–20° N, 90° E–100° E region. Similarly, the red, green and blue curve represents the same for 5° S–5° N, 80° E–100° E; 5° S–15° S, 100° E–120° E; 5° S–15° S, 60° E–90° E (TRIO) regions respectively

Allan RJ, D’Arrigo RD (1999) persistent ENSO sequences: how unusual was the 1990–1995 El Niño? *The Holocene* 9(1):101–118. <https://doi.org/10.1191/095968399669125102>

Allan R, Reason C, Lindesay J, Ansell T (2003) Protracted ENSO episodes and their impacts in the Indian Ocean region. *Deep Sea Res Part II* 50(12–13):2331–2347. [https://doi.org/10.1016/S0967-0645\(03\)00059-6](https://doi.org/10.1016/S0967-0645(03)00059-6)

Balmaseda MA, Mogensen K, Weaver AT (2013) Evaluation of the ecmwf ocean reanalysis system ORAS4. *Q J R Meteorol Soc* 139(674):1132–1161. <https://doi.org/10.1002/qj.2063>

Benthuyzen J, Feng M, Zhong L (2014) Spatial patterns of warming off western australia during the 2011 ningaloo niño: quantifying impacts of remote and local forcing. *Cont Shelf Res* 91:232–246. <https://doi.org/10.1016/j.csr.2014.09.014>

Birol F, Morrow R (2001) Source of the baroclinic waves in the south-east Indian Ocean. *J Geophys Res Oceans* 106(C5):9145–9160. <https://doi.org/10.1029/2000JC900044>

Chen Z, Wen Z, Wu R, Du Y (2017) Roles of tropical SST anomalies in modulating the western north Pacific anomalous cyclone during

- strong La Niña decaying years. *Clim Dyn* 49:633–647. <https://doi.org/10.1007/s00382-016-3364-4>
- Chen Z, Du Y, Wen Z, Wu R, Xie S-P (2019) Evolution of south Tropical Indian Ocean WARMING and the climatic impacts following strong El Niño events. *J Clim* 32(21):7329–7347. <https://doi.org/10.1175/JCLI-D-18-0704.1>
- Cheng L, Zheng F, Zhu J (2015) Distinctive ocean interior changes during the recent warming slowdown. *Sci Rep* 5(1):1–11. <https://doi.org/10.1038/srep14346>
- Chowdary JS, Gnanaseelan C (2007) Basin-wide warming of the Indian Ocean during El Niño and Indian ocean dipole years. *Int J Climatol* 27(11):1421–1438. <https://doi.org/10.1002/joc.1482>
- Chowdary JS, Gnanaseelan C, Vaid B, Salvekar P (2006) Changing trends in the tropical Indian Ocean SST during La Niña years. *Geophys Res Lett*. <https://doi.org/10.1029/2006GL026707>
- Clarke AJ, Liu X (1993) Observations and dynamics of semiannual and annual sea levels near the eastern equatorial Indian Ocean boundary. *J Phys Oceanogr* 23(2):386–399. [https://doi.org/10.1175/1520-0485\(1993\)023%3c0386:OADOSA%3e2.0.CO;2](https://doi.org/10.1175/1520-0485(1993)023%3c0386:OADOSA%3e2.0.CO;2)
- Deepa JS, Gnanaseelan C, Kakatkar R, Parekh A, Chowdary JS (2018) The interannual sea level variability in the Indian ocean as simulated by an ocean general circulation model. *Int J Climatol* 38(3):1132–1144. <https://doi.org/10.1002/joc.5228>
- Deepa JS, Gnanaseelan C, Mohapatra S, Chowdary JS, Karmakar A, Kakatkar R, Parekh A (2019) The tropical Indian Ocean decadal sea level response to the pacific decadal oscillation forcing. *Clim Dyn* 52(7–8):5045–5058. <https://doi.org/10.1007/s00382-018-4431-9>
- Du Y, Xie SP, Huang G, Hu K (2009) Role of air–sea interaction in the long persistence of El Niño–induced north indian ocean warming. *J Clim* 22(8):2023–2038. <https://doi.org/10.1175/2008JCLI2590.1>
- Du Y, Cai W, Wu Y (2013) A new type of the indian ocean dipole since the mid-1970s. *J Clim* 26(3):959–972. <https://doi.org/10.1175/JCLI-D-12-00047.1>
- England MH, Huang F (2005) On the interannual variability of the Indonesian throughflow and its linkage with ENSO. *J Clim* 18(9):1435–1444. <https://doi.org/10.1175/JCLI3322.1>
- England MH, McGregor S, Spence P, Meehl GA, Timmermann A, Cai W, Gupta AS, McPhaden MJ, Purich A, Santoso A (2014) Recent intensification of wind-driven circulation in the pacific and the ongoing warming hiatus. *Nat Clim Change* 4(3):222–227. <https://doi.org/10.1038/nclimate2106>
- Gnanaseelan C, Deshpande A, McPhaden MJ (2012) Impact of Indian Ocean Dipole and El Niño/Southern Oscillation forcing on the Wyrki jets. *J Geophys Res Oceans* 117:C08005. <https://doi.org/10.1029/2012JC007918>
- Godfrey J (1996) The effect of the Indonesian Throughflow on ocean circulation and heat exchange with the atmosphere: a review. *J Geophys Res Oceans* 101(C5):12217–12237. <https://doi.org/10.1029/95JC03860>
- Han W, Vialard J, McPhaden MJ, Lee T, Masumoto Y, Feng M, De Ruijter WP (2014) Indian Ocean decadal variability: A review. *Bull Am Meteor Soc* 95(11):1679–1703. <https://doi.org/10.1175/BAMS-D-13-00028.1>
- Hastenrath S, Lamb P (1979) Climatic atlas of the Indian Ocean, part 2, the ocean heat budget. University of Wisconsin Press, Madison
- Hastenrath S, Nicklis A, Greischar L (1993) Atmospheric-hydrospheric mechanisms of climate anomalies in the western equatorial Indian Ocean. *J Geophys Res Oceans* 98(C11):20219–20235. <https://doi.org/10.1029/93JC02330>
- He S, Yu JY, Yang S, Fang SW (2020) ENSOs impacts on the tropical Indian and atlantic oceans via tropical atmospheric processes: observations versus cmip5 simulations. *Clim Dyn* 54(11):4627–4640. <https://doi.org/10.1007/s00382-020-05247-w>
- Karmakar A, Parekh A, Chowdary JS, Gnanaseelan C (2018) Inter comparison of tropical Indian Ocean features in different ocean reanalysis products. *Clim Dyn* 51(1–2):119–141. <https://doi.org/10.1007/s00382-017-3910-8>
- Klein SA, Soden BJ, Lau NC (1999) Remote sea surface temperature variations during ENSO: evidence for a tropical atmospheric bridge. *J Clim* 12(4):917–932. [https://doi.org/10.1175/1520-0442\(1999\)012%3c0917:RSSTVD%3e2.0.CO;2](https://doi.org/10.1175/1520-0442(1999)012%3c0917:RSSTVD%3e2.0.CO;2)
- Kosaka Y, Xie SP (2013) Recent global-warming hiatus tied to equatorial pacific surface cooling. *Nature* 501(7467):403–407. <https://doi.org/10.1038/nature12534>
- Lee SK, Park W, Baringer MO, Gordon AL, Huber B, Liu Y (2015) Pacific origin of the abrupt increase in Indian Ocean heat content during the warming hiatus. *Nat Geo-Sci* 8(6):445–449. <https://doi.org/10.1038/ngeo2438>
- Li Y, Han W, Hu A, Meehl GA, Wang F (2018) Multidecadal changes of the upper Indian Ocean heat content during 1965–2016. *J Clim* 31(19):7863–7884. <https://doi.org/10.1175/JCLI-D-18-0116.1>
- Li Y, Han W, Zhang L, Wang F (2019) Decadal SST variability in the southeast Indian Ocean and its impact on regional climate. *J Clim* 32(19):6299–6318. <https://doi.org/10.1175/JCLI-D19-0180.1>
- Liu W, Xie SP, Lu J (2016) Tracking ocean heat uptake during the surface warming hiatus. *Nat Commun* 7(1):1–9. <https://doi.org/10.1038/ncomms10926>
- Luyten JR, Roemmich DH (1982) Equatorial currents at semi-annual period in the Indian ocean. *J Phys Oceanogr* 12(5):406–413. [https://doi.org/10.1175/1520-0485\(1982\)012%3c0406:ECASAP%3e2.0.CO;2](https://doi.org/10.1175/1520-0485(1982)012%3c0406:ECASAP%3e2.0.CO;2)
- Ma J, Feng M, Sloyan BM, Lan J (2019) Pacific influences on the meridional temperature transport of the Indian Ocean. *J Clim* 32(4):1047–1061. <https://doi.org/10.1175/JCLI-D-18-0349.1>
- Masumoto Y, Meyers G (1998) Forced rossby waves in the southern tropical Indian Ocean. *J Geophys Res Oceans* 103(C12):27589–27602. <https://doi.org/10.1029/98JC02546>
- Meehl GA, Arblaster JM, Fasullo JT, Hu A, Trenberth KE (2011) Model-based evidence of deepocean heat uptake during surface-temperature hiatus periods. *Nat Clim Change* 1(7):360–364. <https://doi.org/10.1038/nclimate1229>
- Meyers G (1996) Variation of Indonesian throughflow and the El Niño Southern Oscillation. *J Geophys Res Oceans* 101(C5):12255–12263. <https://doi.org/10.1029/95JC03729>
- Miyama T, McCreary JP Jr, Jensen TG, Loschnigg J, Godfrey S, Ishida A (2003) Structure and dynamics of the indian-ocean cross-equatorial cell. *Deep Sea Res Part II* 50(12–13):2023–2047. [https://doi.org/10.1016/S09670645\(03\)00044-4](https://doi.org/10.1016/S09670645(03)00044-4)
- Nieves V, Willis JK, Patzert WC (2015) Recent hiatus caused by decadal shift in indo-pacific heating. *Science* 349(6247):532–535. <https://doi.org/10.1126/science.aaa4521>
- Parekh A, Gnanaseelan C, Jayakumar A (2011) Impact of improved momentum transfer coefficients on the dynamics and thermodynamics of the North Indian Ocean. *J Geophys Res Oceans*. <https://doi.org/10.1029/2010JC006346>
- Rahul S, Gnanaseelan C (2016) Can large scale surface circulation changes modulate the sea surface warming pattern in the tropical Indian Ocean? *Clim Dyn* 46(11):3617–3632. <https://doi.org/10.1007/s00382-015-2790-z>
- Rao R (1986) Cooling and deepening of the mixed layer in the central Arabian Sea during monsoon77: observations and simulations. *Deep Sea Res Part A Oceanogr Res Pap* 33(10):1413–1424. [https://doi.org/10.1016/0198-0149\(86\)90043-9](https://doi.org/10.1016/0198-0149(86)90043-9)
- Reason C, Allan R, Lindesay J, Ansell T (2000) ENSO and climatic signals across the Indian Ocean basin in the global context: part I, interannual composite patterns. *Int J Clim* 20(11):1285–1327. [https://doi.org/10.1002/1097-0088\(200009\)20:11%3c1285::AID-JOC536%3e3.0.CO;2-R](https://doi.org/10.1002/1097-0088(200009)20:11%3c1285::AID-JOC536%3e3.0.CO;2-R)

- Saji NH, Goswami BN, Vinayachandran PN, Yamagata T (1999) A dipole mode in the tropical Indian Ocean. *Nature* 401:360–363
- Sayantani O, Gnanaseelan C (2015) Tropical Indian Ocean subsurface temperature variability and the forcing mechanisms. *Clim Dyn* 44(9–10):2447–2462. <https://doi.org/10.1007/s00382-014-2379-y>
- Schott FA, Xie S, McCreary JP (2009) Indian Ocean circulation and climate variability. *Rev Geophys*. <https://doi.org/10.1029/2007RG000245>
- Singh P, Chowdary JS, Gnanaseelan C (2013) Impact of prolonged La Niña/La Niña events on the Indian Ocean with a special emphasis on southwest tropical Indian Ocean sst. *Global Planet Change* 100:28–37. <https://doi.org/10.1016/j.gloplacha.2012.10.010>
- Sprintall J, Revelard A (2014) The Indonesian throughflow response to indo-pacific climate variability. *J Geophys Res Oceans* 119(2):1161–1175. <https://doi.org/10.1002/2013JC009533>
- Sprintall J, Wijffels SE, Molcard R, Jaya I (2009) Direct estimates of the Indonesian through-flow entering the Indian Ocean: 2004–2006. *J Geophys Res Oceans*. <https://doi.org/10.1029/2008JC005257>
- Sreenivas P, Gnanaseelan C, Prasad KVS (2012) Influence of El Nino and Indian Ocean Dipole on sea level variability in the Bay of Bengal. *Glob Planet Change* 80–81:215–225. <https://doi.org/10.1016/j.gloplacha.2011.11.001>
- Srinivas G, Chowdary JS, Gnanaseelan C, Prasad K, Karmakar A, Parekh A (2018) Association between mean and interannual equatorial Indian Ocean subsurface temperature bias in a coupled model. *Clim Dyn* 50(5–6):1659–1673. <https://doi.org/10.1007/s00382-017-3713-y>
- Srinivasu U, Ravichandran M, Han W, Sivareddy S, Rahman H, Li Y, Nayak S (2017) Causes for the reversal of north Indian Ocean decadal sea level trend in recent two decades. *Clim Dyn* 49(11–12):3887–3904. <https://doi.org/10.1007/s00382-017-3551-y>
- Thompson PR, Piecuch CG, Merrifield MA, McCreary JP, Firing E (2016) Forcing of recent decadal variability in the equatorial and north Indian Ocean. *J Geophys Res Oceans* 121(9):6762–6778. <https://doi.org/10.1002/2016JC012132>
- Trenary LL, Han W (2012) Intraseasonal-to-interannual variability of south Indian Ocean sea level and thermocline: remote versus local forcing. *J Phys Oceanogr* 42(4):602–627. <https://doi.org/10.1175/JPO-D-11-084.1>
- Vaid B, Gnanaseelan C, Polito P, Salvekar PS (2007) Influence of Pacific on Southern Indian Ocean Rossby waves. *Pure Appl Geophys* 164(8):1765–1785. <https://doi.org/10.1007/s00024-007-0230-7>
- Verschell M, Kindle J, O'Brien JJ (1995) Effects of Indo-Pacific through-flow on the upper tropical pacific and Indian Oceans. *J Geophys Res Oceans* 100(C9):18409–18420. <https://doi.org/10.1029/95JC02075>
- Vinayachandran P, Nanjundiah RS (2009) Indian ocean sea surface salinity variations in a coupled model. *Clim Dyn* 33(2–3):245–263. <https://doi.org/10.1007/s00382-008-0511-6>
- Wijffels S, Meyers G (2004) An intersection of oceanic waveguides: variability in the Indonesian throughflow region. *J Phys Oceanogr* 34(5):1232–1253. [https://doi.org/10.1175/1520-0485\(2004\)034%3c1232:AIOOWV%3e2.0.CO;2](https://doi.org/10.1175/1520-0485(2004)034%3c1232:AIOOWV%3e2.0.CO;2)
- Wu B, Li T, Zhou T (2010) Relative contributions of the Indian Ocean and local SST anomalies to the maintenance of the western north pacific anomalous anticyclone during the el niño decaying summer. *J Clim* 23(11):2974–2986. <https://doi.org/10.1175/2010JCLI3300.1>
- Wyrtki K (1973) An equatorial jet in the Indian Ocean. *Science* 181(4096):262–264. <https://doi.org/10.1126/science.181.4096.262>
- Xie SP, Annamalai H, Schott FA, McCreary JP Jr (2002) Structure and mechanisms of south Indian Ocean climate variability. *J Clim* 15(8):864–878. [https://doi.org/10.1175/1520-0442\(2002\)015%3c0864:SAMOSI%3e2.0.CO;2](https://doi.org/10.1175/1520-0442(2002)015%3c0864:SAMOSI%3e2.0.CO;2)
- Xie SP, Hu K, Hafner J, Tokinaga H, Du Y, Huang G, Sampe T (2009) Indian Ocean capacitor effect on indo-western pacific climate during the summer following El Niño. *J Clim* 22(3):730–747. <https://doi.org/10.1175/2008JCLI2544.1>
- Xie SP, Kosaka Y, Du Y, Hu K, Chowdary JS, Huang G (2016) Indo-western pacific ocean capacitor and coherent climate anomalies in post-ENSO summer: a review. *Adv Atmos Sci* 33(4):411–432. <https://doi.org/10.1007/s00376-015-5192-6>
- Yamagata T, Mizuno K, Masumoto Y (1996) Seasonal variations in the equatorial Indian ocean and their impact on the Lombok through-flow. *J Geophys Res Oceans* 101(C5):12465–12473. <https://doi.org/10.1029/95JC03623>
- Yoshida K (1960) A theory of the cromwell current (the equatorial undercurrent) and of the equatorial upwelling an interpretation in a similarity to a coastal circulation. *J Oceanogr Soci Japan* 15(4):159–170. <https://doi.org/10.5928/kaiyou1942.15.159>
- Zhang Y, Feng M, Du Y, Phillips HE, Bindoff NL, McPhaden MJ (2018) Strengthened Indonesian throughflow drives decadal warming in the southern Indian Ocean. *Geophys Res Lett* 45(12):6167–6175. <https://doi.org/10.1029/2018GL078265>
- Zhang L, Han W, Li Y, Lovenduski NS (2019) Variability of sea level and upper-ocean heat content in the indian ocean: Effects of subtropical Indian Ocean Dipole and ENSO. *J Clim* 32(21):7227–7245. <https://doi.org/10.1175/JCLI-D-19-0167.1>

Publisher's Note Springer Nature remains neutral with regard to jurisdictional claims in published maps and institutional affiliations.